



HAL
open science

Computer simulation of reactions between an edge dislocation and glissile self-interstitial clusters in iron

David John Bacon, Yuri Osetsky, Zhouwen Rong

► **To cite this version:**

David John Bacon, Yuri Osetsky, Zhouwen Rong. Computer simulation of reactions between an edge dislocation and glissile self-interstitial clusters in iron. *Philosophical Magazine*, 2006, 86 (25-26), pp.3921-3936. 10.1080/14786430600570527. hal-00513659

HAL Id: hal-00513659

<https://hal.science/hal-00513659>

Submitted on 1 Sep 2010

HAL is a multi-disciplinary open access archive for the deposit and dissemination of scientific research documents, whether they are published or not. The documents may come from teaching and research institutions in France or abroad, or from public or private research centers.

L'archive ouverte pluridisciplinaire **HAL**, est destinée au dépôt et à la diffusion de documents scientifiques de niveau recherche, publiés ou non, émanant des établissements d'enseignement et de recherche français ou étrangers, des laboratoires publics ou privés.



Computer simulation of reactions between an edge dislocation and glissile self-interstitial clusters in iron

Journal:	<i>Philosophical Magazine & Philosophical Magazine Letters</i>
Manuscript ID:	TPHM-05-Oct-0441.R1
Journal Selection:	Philosophical Magazine
Date Submitted by the Author:	22-Dec-2005
Complete List of Authors:	Bacon, David; University of Liverpool, Engineering Osetsky, Yuri; Oak Ridge National Laboratory, Computer Science and Mathematics Division Rong, Zhouwen; University of Liverpool, Engineering
Keywords:	radiation damage, computer simulation, dislocation dynamics, plasticity of metals, point defects
Keywords (user supplied):	dislocation loop, iron, interstitial cluster



1
2
3
4
5
6
7
8
9
10
11
12
13
14
15
16
17
18
19
20
21
22
23
24
25
26
27
28
29
30
31
32
33
34
35
36
37
38
39
40
41
42
43
44
45
46
47
48
49
50
51
52
53
54
55
56
57
58
59
60

Computer simulation of reactions between an edge dislocation and glissile self-interstitial clusters in iron

D.J. Bacon¹, Yu.N. Osetsky² and Z.Rong¹

- ¹) Materials Science and Engineering, Department of Engineering,
The University of Liverpool, Liverpool L69 3GH, UK.
²) Computer Science and Mathematics Division,
Oak Ridge National Laboratory,
P. O. Box 2008, Oak Ridge, TN 37831-6158, USA.

ABSTRACT

Clusters of self-interstitial atoms (SIAs) are formed in metals by high-energy displacement cascades, often in the form of small dislocation loops with a perfect Burgers vector, \mathbf{b} . Atomic-scale computer simulation is used here to investigate their reaction with an edge dislocation gliding in α -iron under stress for the situation where \mathbf{b} is inclined to the dislocation slip plane. \mathbf{b} of small loops (37 SIAs here) changes spontaneously and the interstitials are absorbed as a pair of superjogs. The line glides forward at critical stress τ_c when one or more vacancies are created and the jogs adopt a glissile form. A large loop (331 SIAs here) reacts spontaneously with the dislocation to form a segment with $\mathbf{b} = \langle 100 \rangle$, which is sessile on the dislocation slip plane, and as applied stress increases the dislocation side arms are pulled into screw orientation. At low temperature (100K), the $\langle 100 \rangle$ segment remains sessile and the dislocation eventually breaks free when the screw dipole arms cross-slip and annihilate. At 300K and above, the segment can glide across the loop and transform it into a pair of superjogs, which become glissile at τ_c . Small loops are weaker obstacles than voids with a similar number of vacancies, large loops are stronger. Irrespective of size, the interaction processes leading to superjogs are efficient for absorption of SIA clusters from slip bands, an effect observed in flow localisation.

Corresponding author: D.J. Bacon (djbacon@liv.ac.uk)

Keywords: Computer simulation, dislocation loop, interstitial cluster, iron, radiation damage

1. Introduction

Exposure of metals to fast-neutron irradiation can cause a substantial increase in yield stress and a reduction in ductility due to the interaction of dislocations with obstacles on or near their slip plane. The obstacles are formed largely by point defect clusters created in displacement cascades. Molecular dynamics (MD) computer simulations have shown that the self-interstitial atom (SIA) component of primary radiation damage is mainly in the form of platelets of closely-packed, parallel crowdions that are equivalent to small, nanometre-scale interstitial dislocation loops with perfect Burgers vector, \mathbf{b} , parallel to the crowdion axis, e.g. [1,2]. Atomistic simulations of a variety of BCC, FCC and HCP metals have shown that such loops are glissile and move in one dimension parallel to the crowdion axis by thermally-activated events with a low activation energy of $\sim 0.02\text{eV}$ [3-5]. They have a long-range strain field and can interact with dislocations by either intersecting their slip plane or gliding to decorate them in regions where they are attracted by the dislocation stress field. The latter possibility has support from experiment, e.g. [6], and modelling, e.g. [7,8]. Further, the interaction of gliding dislocations with loops clearly influences the flow stress and ductility of irradiated metals, and is believed to play an important role in flow localisation and the formation of slip channels that appear to be cleared of radiation damage debris [9].

Decoration of dislocation sources by ‘atmospheres’ of interstitial loops led Singh and co-workers [10] to argue that the increase in the upper yield stress and the subsequent yield drop are related to the stress necessary to unlock dislocations from the loops that decorate them. Estimates of the unlocking stress for a straight dislocation were found to be consistent with experiment. A continuum dislocation dynamics method was later used to determine the stress for a flexible dislocation to break away from rows of loops below the slip plane and confirmed the earlier estimates [11,12]. These treatments assumed the interstitial loops to be static and unable to glide with a dislocation, whereas perfect loops are intrinsically glissile and those nearest the slip plane not only exert the largest force on the dislocation but also experience the largest force tending to make them glide. This was pointed out by Makin [13], who calculated the long-range elastic interaction between a dislocation and loop and noted that loops lying close to the glide plane of a dislocation

1
2
3
4 with the same \mathbf{b} may be swept along with it, although the effect could not be quantified in
5
6 the absence of information on the force to move a loop at the atomic scale.
7

8 The present work is part of a series of atomic-scale studies of the dynamics of
9 dislocation behaviour in the presence of interstitial loops in α -iron (Fe). Loops with $\mathbf{b} =$
10 $\frac{1}{2}\langle 111 \rangle$ and $\langle 100 \rangle$ grow during irradiation of this metal. The origin of the latter, which
11 have the larger elastic energy, is unclear. It has been proposed that both sets could result by
12 shear from a common $\frac{1}{2}\langle 110 \rangle$ nucleus [14], or that two intersecting $\frac{1}{2}\langle 111 \rangle$ clusters can
13 react to form a $\langle 100 \rangle$ loop [15]. However, neither mechanism has yet been demonstrated
14 to occur and the $\frac{1}{2}\langle 111 \rangle$ configuration has lower energy than $\langle 100 \rangle$ using all currently
15 available interatomic potentials. Since $\frac{1}{2}\langle 111 \rangle$ SIA clusters arise in irradiated iron and
16 other BCC metals, we have concentrated on them in the first part of this study. In any
17 case, it is not obvious *a priori* which creates the stronger obstacle to glide of a dislocation
18 with $\mathbf{b} = \frac{1}{2}\langle 111 \rangle$ because the dislocation can react favourably with a $\frac{1}{2}\langle 111 \rangle$ loop to form
19 a $\langle 100 \rangle$ segment, which can be sessile (see later), whereas the favourable reaction with a
20 $\langle 100 \rangle$ loop results in another $\frac{1}{2}\langle 111 \rangle$ segment, which is glissile. Thus, both loop types
21 need to be studied and we will report on treatment of $\langle 100 \rangle$ loops in a second part.
22
23
24
25
26
27
28
29
30
31
32

33 Previously, the interaction of a $\frac{1}{2}\langle 111 \rangle\{110\}$ edge dislocation gliding under
34 applied stress with sets of $\frac{1}{2}\langle 111 \rangle$ SIA clusters of size $\sim 1\text{nm}$ distributed below the extra
35 half-plane was simulated for a range of temperature [16,17]. It was found that a row of
36 loops can be dragged at almost the free-flight velocity of the dislocation ($\sim 100\text{ms}^{-1}$ for
37 10MPa at 300K). A quantitative model for this, based on a drag coefficient derived from
38 the diffusivity of interstitial loops, was presented, and the conditions under which a
39 dislocation breaks away from a row of glissile loops was determined. Perfect dislocation
40 loops in this metal have \mathbf{b} equal to one of the four possible vectors $\frac{1}{2}\langle 111 \rangle$, but only two
41 of them are parallel to the $\{110\}$ slip plane of a dislocation and were considered for drag.
42 Glissile loops with one of the other two \mathbf{b} s can move to intersect the dislocation glide
43 plane, however, and cause direct dislocation-dislocation reaction. This latter process is
44 modelled in the present work and its dependence on temperature, T , applied shear strain
45 rate, $\dot{\epsilon}$, and loop size analysed. We have again considered the edge dislocation.
46
47
48
49
50
51
52
53
54
55

56 Although it is well known that glide of screw dislocations controls slip in BCC
57 metals at low T , it should be noted that edge dislocations have to interact/absorb/overcome
58 loops for plastic flow to occur at any temperature. Their mechanisms therefore have to be
59
60

1
2
3
4 investigated since there is no reason to suppose *a priori* that they are not important.
5
6 Furthermore, dislocation glide can result in the production of cleared channels, as noted
7
8 above, and, although some static and dynamic simulations of screw- $1/2\langle 111 \rangle$ loop
9
10 interaction have been reported [18,19], we are not aware of evidence that screw
11
12 dislocations absorb/remove loops to result in clear band formation.

13
14 The method employed here is summarised in section 2 and the results presented in
15
16 section 3. Section 4 contains a discussion of the investigation, including an assessment of
17
18 its consequences for understanding the effects of irradiation on plasticity in iron. We also
19
20 compare the present results with those of a very recent MD simulation of dislocation-loop
21
22 interaction in iron with the same geometry as used here by Nomoto et al. [20] and with a
23
24 qualitatively similar study of dislocation-loop interaction in the FCC metal nickel by
25
26 Rodney and Martin [21,22].

27 28 2. Method and geometry

29
30
31 The method developed by Osetsky and Bacon [23], which treats a periodic array of
32
33 edge dislocations, was employed. The x , y and z axes of the simulated crystal were
34
35 oriented along $[111]$, $[\bar{1}\bar{1}2]$ and $[1\bar{1}0]$ directions, as illustrated in Fig. 1. Periodic
36
37 boundary conditions were employed in the x and y directions, corresponding to the
38
39 direction of \mathbf{b} and the line direction, respectively, and fixed conditions were used across the
40
41 z boundaries. Choice of crystal dimensions is important for modelling dislocation motion
42
43 because the size, L_x , along the x -axis should be large enough for interactions between the
44
45 dislocation and its images to be insignificant [23]. We used $L_x = 120b$ ($\sim 29.8\text{nm}$ for Fe with
46
47 model lattice parameter $a_0 = 0.2867\text{nm}$ at temperature $T = 0\text{K}$); the period, L_y , defines the
48
49 inter-cluster spacing and was $59\sqrt{6}a_0$ ($\sim 41.4\text{nm}$); and L_z was $49\sqrt{2}a_0$ ($\sim 19.9\text{nm}$). The total
50
51 number of mobile atoms in the MD cell was $\sim 2.1\text{M}$.

52
53 Rigid blocks of atoms were used at the z -axis boundaries to apply shear strain, ϵ , by
54
55 displacement of the $+z$ block. The corresponding applied shear stress, τ ($= \tau_{xz}$), was
56
57 computed from the shear force on this block due to the free atoms of the inner region (see
58
59 [23]). Molecular statics (MS) relaxation, i.e. potential energy minimisation, was used to
60
simulate athermal loading at $T = 0\text{K}$ under strain increasing in increments $\Delta\epsilon = 2$ to 10×10^{-5} .
Molecular dynamics (MD) with timestep 2-5fs was used for constant-strain-rate

1
2
3
4 deformation at $T > 0K$, with $\dot{\epsilon}$ in the range $2-100 \times 10^6 s^{-1}$ and T in the range $100-450K$, as
5 defined by the mean atomic kinetic energy. Thermal expansion was treated by changing a_0
6 until the total pressure fluctuated around zero.
7
8

9
10 The Finnis-Sinclair-type interatomic potential for Fe of Ackland et al. [24] was
11 used. The SIA clusters/loops were created in the model by inserting $\langle 111 \rangle$ dumbbells
12 after the dislocation had been formed and relaxed, and then relaxing the model again to
13 minimise the potential energy. They contained N interstitials and were of hexagonal shape
14 with sides of length $d = a_0(2N)^{1/2}/3$ along $\langle 112 \rangle$ directions. Values $N = 37$ and 331 were
15 chosen, i.e. $d = 0.82$ and $2.46nm$, respectively. The centre of the cluster was positioned a
16 distance H below the slip plane, as depicted in figure 1. Values of H equal to 11 , 22 and
17 $33a_0$ were used. The two loop Burgers vectors $\frac{1}{2}[1\bar{1}1]$ and $\frac{1}{2}[\bar{1}11]$ are inclined to the
18 $(1\bar{1}0)$ slip plane, but they are symmetric with respect to the dislocation, so only one need
19 be considered. A loop with $\mathbf{b} = \frac{1}{2}[1\bar{1}1]$ is shown schematically in Fig. 1.
20
21
22
23
24
25
26
27
28
29

30 3. Results

31 3.1. Reaction at $T = 0K$

32
33 Under the attractive field of the dislocation, and even in the absence of thermal
34 motion of the atoms, small SIA loops glide over the H range considered to meet the
35 dislocation as it moves under strain on its slip plane. (The thickness of cleared channels
36 was not a concern of this work, but the band of interaction over which loops can glide to an
37 edge dislocation must at least $33a_0$, even at $T = 0K$. It was not feasible to model larger
38 crystals to investigate this dimension further.) The dislocation actually bows forward as a
39 loop approaches in order to assist the favourable reaction. Fig. 2(a) shows a visualisation
40 of the initial dislocation line and 37-SIA cluster viewed from the front of the model crystal
41 in Fig. 1. The dislocation has already started to bow forward slightly and as it moves
42 further under the applied strain the loop slips on its glide cylinder along $[1\bar{1}1]$ to meet it.
43 The axis of the crowdions then changes to $[111]$, i.e. \mathbf{b} of the SIA loop rotates to be the
44 same as that of the dislocation line. The newly-formed pair of superjogs restricts the slip
45 of the dislocation (Fig. 2(b)) until the SIAs that form it reorganise by self-climb and
46 emission of a vacancy in the crystal to give glissile segments on $\{110\}$ or $\{112\}$ planes of
47
48
49
50
51
52
53
54
55
56
57
58
59
60

1
2
3
4 the [111] zone axis, as seen in Fig. 2(c). The jogged dislocation then continues to glide
5 with little hindrance.
6
7

8 The relationship between τ and ϵ during the process is plotted in Fig. 3. In the
9 absence of any other defect, the edge dislocation glides on a $\{110\}$ plane in the model at T
10 = 0K under applied resolved shear stress of about 25MPa [23]: this is the Peierls stress, τ_p .
11 As the dislocation approaches the periodic row of SIA clusters, it is initially attracted
12 towards them ($\tau < \tau_p$) and becomes pinned by the double superjogs formed by the reaction.
13 τ rises as ϵ increases until reaching a maximum (i.e. critical) stress $\tau_c = 51\text{MPa}$, at which
14 stage a vacancy is created and the superjogs become glissile on the $\mathbf{b} = \frac{1}{2}[111]$ system and
15 τ falls to τ_p . The process described does not depend on the increment $\Delta\epsilon$ used here, as seen
16 from the two sets of data in Fig. 3.
17
18
19
20
21
22
23

24 The simulations for $T = 0\text{K}$ provide information on the equilibrium (minimum
25 potential energy) structure at each strain increment, and the configurations are equivalent
26 to those that would be obtained by minimising the elastic energy in the continuum
27 approximation. However, they do not necessarily reveal information about the atomic
28 mechanisms that would occur in a real metal where thermal effects assist the reaction
29 process. For this reason, most modelling has been done using MD, as described in the
30 following section.
31
32
33
34
35
36
37

38 **3.2. Reaction at $T > 0\text{K}$**

39 **3.2.1. Small loops**

40
41
42 The aim of this part of the study was to examine the effect of cluster size,
43 temperature and $\dot{\epsilon}$ on the reaction and strengthening mechanism. The 37-SIA cluster is
44 considered first. Its interaction with the edge dislocation has been investigated for $T =$
45 100, 300 and 450K in a model with applied $\dot{\epsilon}$ values in the range $2\text{-}10 \times 10^6 \text{s}^{-1}$. (For the
46 dislocation density $(L_x L_z)^{-1}$ used here, this corresponds to dislocation velocity in steady
47 state of $5\text{-}24 \text{ms}^{-1}$.) Under all conditions considered, the cluster glides to meet the
48 dislocation and the axis of its crowdions rotates from $[1\bar{1}1]$ to $[111]$ when the cores of the
49 two defects react. This results in creation of a pair of superjogs, which hinders slip of the
50 dislocation and results in increasing τ until the interstitials in the superjogs reorganise by
51 emitting a vacancy and form glissile segments on slip planes of the $[111]$ zone. The
52
53
54
55
56
57
58
59
60

1
2
3
4 before-and-after structures are the same as those for $T = 0\text{K}$ in Fig. 2. Unsurprisingly, the
5 critical stress, τ_c , is less than at 0K . This is illustrated by the τ versus ϵ and time, t , plot for
6 $T = 100\text{K}$ and $\dot{\epsilon} = 2 \times 10^6 \text{s}^{-1}$ included in Fig. 3. The noise in the plot arises because of the
7 non-zero temperature, but it can be seen that the dislocation, which glides at a stress of
8 only a few MPa at this T and $\dot{\epsilon}$, is initially attracted to the loop ($\tau < 0$), is then held back by
9 the superjogs and eventually at $t \sim 0.8\text{ns}$ glides forward when the $\frac{1}{2}[111]$ superjogs
10 become glissile: this final step takes place at a smaller stress (26MPa) and strain than at
11 0K .

12
13 The data for τ_c for the various conditions of T and $\dot{\epsilon}$ are plotted in Fig. 4. It is seen
14 that τ_c is almost independent of both parameters when $T > 0\text{K}$. Visualisation of the defect
15 configuration during the loop transformation shows that rotation of \mathbf{b} does not occur until
16 the cores of the dislocation and loop meet. Furthermore, it is not the process that controls
17 τ_c , for τ continues to increase beyond this rotation stage. Glide of the dislocation and
18 absorbed loop occurs when atoms in segments of the core of the transformed loop re-
19 arrange at τ_c to form glissile superjogs.

3.2.2. Large loops

20
21
22
23
24
25
26
27
28
29
30
31
32
33
34
35
36
37
38
39
40
41
42
43
44
45
46
47
48
49
50
51
52
53
54
55
56
57
58
59
60
Loops containing 37 SIAs are typical of those formed directly in the primary
displacement cascade process, which is consistent with the mean size $\sim 1\text{nm}$ observed
experimentally at low irradiation dose ($\sim 10^{-3}\text{dpa}$) [25-27]. These loops are highly mobile
and can move by mutual attraction to form larger dislocation loops, as seen in MD
simulations [28] and, therefore, loop size increases with irradiation dose, reaching $\sim 5\text{nm}$ at
 $\sim 1\text{dpa}$ [25-27]. Thus, we now consider loops containing 331 interstitials; they have $d =$
 2.46nm , which is equivalent to diameter $\sim 5\text{nm}$.

Five frames showing the interaction at 300K for $\dot{\epsilon} = 20 \times 10^6 \text{s}^{-1}$ are presented in Fig.
5. Initially, the loop glides towards the dislocation glide plane and its upper segment
attracts the dislocation, which bows forward (Fig. 5(a)). When they meet (Fig. 5(b)), the
Burgers vector of the upper segment is transformed by the reaction

$$\frac{1}{2}[111] + \frac{1}{2}[\bar{1}\bar{1}\bar{1}] = [010], \quad (1)$$

which is energetically-favourable according to Frank's rule. The remainder of the initial
loop retains its $\frac{1}{2}[1\bar{1}\bar{1}]$ Burgers vector. The $[010]$ segment is sessile in the $(1\bar{1}0)$ slip

1
2
3
4
5
6
7
8
9
10
11
12
13
14
15
16
17
18
19
20
21
22
23
24
25
26
27
28
29
30
31
32
33
34
35
36
37
38
39
40
41
42
43
44
45
46
47
48
49
50
51
52
53
54
55
56
57
58
59
60

plane of the dislocation, but glissile in the inclined (101) plane. However, it is pinned at its ends by the junctions with the $\frac{1}{2}[111]$ and $\frac{1}{2}[\bar{1}\bar{1}\bar{1}]$ lines, and is too short to bow under the applied stress. As τ increases, the $\frac{1}{2}[111]$ line segments pinned at the junctions are pulled into the screw orientation (Fig. 5(c)) and, assisted by the applied force on the [010] segment, cross-slip on $(10\bar{1})$ planes, thereby allowing the [010] segment to slip downwards on the (101) plane. This is shown in the view along $[\bar{1}\bar{1}\bar{1}]$ in Fig. 5(d). Eventually, at high enough applied stress, the downwards slip of the [010] dislocation and the [111] screw side arms completes the transformation of the loop into a pair of $\frac{1}{2}[111]$ superjogs on the gliding dislocation, wherein all 331 SIAs are contained (Fig. 5(e)). A few vacancies are formed in the crystal at the point when the dislocation glides forward at τ_c , in a similar manner to the small loop above, resulting in additional SIAs in the jogs. The reaction and transformation is completed in less than 0.8ns at this strain rate. It is shown in schematic representation in Fig. 6. The arrows denoting the direction of \mathbf{b} are obtained using the RH/FS convention with the positive line sense indicated [29].

The maximum stress, τ_c , for the process in Fig. 5 is 220MPa and the jogged dislocation line continues to glide at $\tau = 12\text{MPa}$. The same reaction and transformation process occurred for the other two $\dot{\epsilon}$ at 300K and at 450K. The value of τ_c depends on T and $\dot{\epsilon}$, however, as shown by the data plotted in Fig. 4. The interaction was also simulated for $T = 450\text{K}$ and $\dot{\epsilon} = 5 \times 10^6 \text{s}^{-1}$, but with the sense of the applied strain reversed, i.e. the dislocation approached the loop from the right-hand side of the model in the schematic illustration of Fig. 1. The critical stress was the same as that in Fig. 4 and the transformation and unpinning processes were unchanged.

The interaction at 100K and $\dot{\epsilon} = 5 \times 10^6 \text{s}^{-1}$ resulted in $\tau_c = 290\text{MPa}$ (see Fig. 4) and had a different outcome. Two frames in the process are shown in Fig. 7. Creation of a [010] segment by the reaction of eq. (1) occurred again (Fig. 7(a)), but the segment was seen to be sessile in the loop plane at this low temperature and a long screw dipole formed on the $\frac{1}{2}[111]$ dislocation under increasing stress (Fig. 7(b)). The dipole eventually annihilated by cross-slip of its arms, which has started in Fig. 7(b), and the $\frac{1}{2}[1\bar{1}\bar{1}]$ loop was restored. Thus, both the strength of large loops and the ease with which they are absorbed as superjogs depend on temperature via the mobility of $\langle 100 \rangle$ segments.

4. Discussion

1
2
3
4
5
6
7
8
9
10
11
12
13
14
15
16
17
18
19
20
21
22
23
24
25
26
27
28
29
30
31
32
33
34
35
36
37
38
39
40
41
42
43
44
45
46
47
48
49
50
51
52
53
54
55
56
57
58
59
60

This research shows clearly that the interaction mechanism between an edge dislocation and a $\frac{1}{2}\langle 111 \rangle$ interstitial loop whose glide cylinder intersects the dislocation slip plane depends on the size of the loop. Consequently, the obstacle strength provided by a loop against dislocation motion depends on loop size and, for large loops, also changes with temperature and applied $\dot{\epsilon}$. Small loops (37 SIAs here) offer the least resistance because, even in the absence of thermal effects ($T = 0\text{K}$), they are able to undergo rotation of the crowdion axis, \mathbf{b} , on meeting the dislocation and be absorbed on it as a double superjog. (A few simulations have been performed for 61-SIA loops, and the \mathbf{b} -rotation and loop absorption process is the same.) The maximum stress corresponds to the creation of point defects as the core of the jog segments reorganises to become glissile. The superjogs have only a small drag effect on the line after this in both statics and dynamics simulations.

This stress-assisted transformation occurs at $\tau_c = 51\text{MPa}$ at 0K and between 13 and 27MPa at $T > 0\text{K}$ when the inter-loop spacing, L_y , equals 41.4nm. This compares with $\tau_c \sim 100$ and 118 MPa at $T = 0\text{K}$ for an edge dislocation to cut through a row of spherical voids in iron containing a similar number (27 or 59) of vacancies and with the same spacing. Thus, small dislocation loops are relatively weak obstacles compared with voids. Note, however, that all the SIAs are absorbed by the line in the form of a double superjog: only a few vacancies are absorbed by climb when a dislocation passes through a void at $T = 0\text{K}$ [30]. Furthermore, superjogs increase the interaction cross-section of a dislocation for reaction and/or annihilation with other defects in a crystal. Thus, the SIA-loop absorption process should be effective in assisting the creation of defect-free channels when slip occurs in irradiated iron.

This absorption effect for small loops is similar to that found in simulation of edge dislocation-SIA loop interaction in nickel by Rodney and Martin [21,22]. Loops with 4-37 interstitials and a $\langle 110 \rangle$ crowdion axis were absorbed by the dislocation, which is dissociated in the FCC structure, by rotation of their axis (\mathbf{b}). This resulted in either transformation into a pair of superjogs on the dislocation, as here, or attachment to one of the Shockley partials by means of a dislocation junction. Furthermore, recent simulations have shown that rotation of \mathbf{b} also occurs for small clusters of crowdion SIAs gliding into contact with an edge dislocation of the prism-slip system in α -zirconium [31]. This metal

1
2
3
4 has the HCP crystal structure, and so the rotation-absorption process requiring relatively
5 low stress seems quite general for loops with up to a few tens of defects. Note that rotation
6 requires contact interaction with a dislocation: it does not occur for SIA clusters in
7 isolation if they contain more than four or five interstitials [32].
8
9

10
11 The reaction with a large loop (331 SIAs here) provides a much stronger obstacle to
12 dislocation motion than that with a small loop because spontaneous rotation of \mathbf{b} when the
13 two defects first meet does not occur. Instead, a segment with $\mathbf{b} = \langle 100 \rangle$ is formed. It is
14 sessile in the dislocation glide plane and can only glide across the loop plane and complete
15 the transformation to $\mathbf{b} = \frac{1}{2}\langle 111 \rangle$ when, under sufficiently high τ , the dislocation side
16 arms are pulled into screw orientation and then cross-slip (Fig. 6). τ_c is not only much
17 higher but also more strongly temperature-dependent for this process. In fact, glide of the
18 $\langle 100 \rangle$ segment does not occur at 100K, i.e. it is effectively immobile, and the high value
19 of τ_c is controlled by cross-slip and annihilation of the arms of the $\frac{1}{2}\langle 111 \rangle$ screw dipole.
20 In this case, the original loop is restored at dislocation breakaway, rather than absorbed.
21
22
23
24
25
26
27
28
29

30 Unlike the situation for small obstacles, τ_c for 331-SIA loops is higher than for
31 voids with a similar number of vacancies. For example, τ_c equals 150MPa at $\dot{\epsilon} = 5 \times 10^6 \text{s}^{-1}$
32 for spherical voids containing 339 vacancies in iron at 300K with the same spacing as here
33 [30], compared with 212MPa for 331-SIA loops at 300K and 290MPa at 100K, as shown
34 by the τ versus ϵ plots in Fig. 8. Note that the edge dislocation shape at the critical stress τ_c
35 is similar to that in the Orowan mechanism, i.e. a dipole of two parallel screw segments
36 with spacing close to the obstacle size. The effective size for the 331-SIA loop is larger
37 than that for the 339-vacancy void, namely $\sim 5\text{nm}$ compared with $\sim 2\text{nm}$. This is probably
38 the main reason for the higher τ_c value for the 331-SIA loop because τ_c for the Orowan
39 configuration scales roughly as the logarithm of the obstacle size [33].
40
41
42
43
44
45
46
47

48 As with small loops, all the interstitials are absorbed in the pair of glissile
49 superjogs, except at 100K, so the process can be expected to be efficient at removing
50 damage from slip bands. We have not investigated the size, which may be T- and $\dot{\epsilon}$ -
51 dependent, for the transition from small-to-large loop behaviour. Extensive modelling is
52 required and will be the subject of a later paper.
53
54
55

56 Only one line length L_y (= loop separation) is treated here, but results have general
57 applicability for the following reasons. For large loops, where the dislocation side arms
58 bend to the screw orientation, i.e. the line shape is that of the Orowan process (strong
59
60

obstacles), the critical stress is found in continuum self-stress modelling [33] and MD/MS atomic-scale modelling of strengthening [23,30,34] to be proportional to $(1/L_y)$. For small loops that are absorbed by the dislocation, the stress is again proportional to $(1/L_y)$ because the critical step (vacancy creation at the jog) is a localised process. Simple estimates of the stress τ_c required for the length L_y to move forward and do work ($\approx \tau_c b^2 L_y$) to create a vacancy confirm this.

In very recent work, Nomoto et al. [20] have reported MD simulation of the interaction of an edge dislocation with a periodic row of 99-SIA loops in iron with the same Burgers vector orientations as used here. The model size was only a little smaller than the one used here - L_y was 35nm compared with 41nm - and the interatomic potential was the same. The temperature was not given in the paper. The final configuration found after the dislocation had reacted with the loop was the same as found here, viz. glissile superjogs and a few vacancies. However, the transformation mechanism described in [16] is different, for the $\langle 100 \rangle$ dislocation ('bridge') formed initially was observed to split into two $\frac{1}{2}\langle 111 \rangle$ segments that slipped down on the inclined $\{110\}$ plane. (For the orientation used here in Fig. 1, the equivalent process on the (101) plane would be $[010] = \frac{1}{2}[11\bar{1}] + \frac{1}{2}[\bar{1}11]$.) The difference may be due to the different loop size considered or, more likely, the way the crystal was loaded. The model in [20] was deformed by applying a constant shear stress rather than a constant strain rate. At $\tau = 50\text{MPa}$, the dislocation was stopped by the loop and so stress in the range 150 to 650MPa was simulated for loop transformation and absorption. Under these high stress (and therefore high strain rate) conditions, the free-flight velocity of the edge dislocation is in excess of 1000ms^{-1} [18,19], compared with $\sim 12\text{ms}^{-1}$ at, say, $\dot{\epsilon} = 5 \times 10^6\text{s}^{-1}$ in the present work. Thus, the complete process took a few tens of ps in [20], compared with times one to two orders of magnitude longer for the much lower strain rates used here. The process simulated in [20] is strongly affected by kinetic effects such as observed elsewhere for high dislocation velocities [34,35]. Hence, it is not straightforward to compare the atomic mechanisms. Furthermore, critical stress values were not obtained by the procedure used in [20].

Finally, it should be emphasised again that, irrespective of the size of the interacting loop, complete absorption of the interstitials occurs by all but one of the interactions found here. In addition to removing damage from the crystal by this process, the superjogs on the gliding dislocation increase the possibility of dislocation interaction

with other defects. This may enhance absorption of other SIAs or annihilation of vacancy defects. Investigation of this, and analysis of the drag effect such jogs have on slip, will be the subjects of a future paper.

5. Conclusions

- (a) Perfect dislocation loops containing from a few tens to hundreds of self-interstitial atoms in iron lying within a few tens of nm of the slip plane of an edge dislocation can glide to react with the dislocation when the loop Burgers vector, \mathbf{b} , is inclined to the slip plane.
- (b) The Burgers vector of small loops (37 SIAs here) changes spontaneously on contact and the interstitials are absorbed as a pair of superjogs. The line glides forward at critical stress τ_c when one or more vacancies are created and the jogs adopt glissile form.
- (c) τ_c is 51 MPa at $T = 0\text{K}$ and lies between 13 and 27MPa for $100 \leq T \leq 450\text{K}$. These loops are weaker obstacles than voids with a similar number of vacancies.
- (d) A large loop (331 SIAs here) reacts spontaneously with the dislocation to form a segment with $\mathbf{b} = \langle 100 \rangle$, which is sessile on the dislocation slip plane, and as τ increases the dislocation side arms are pulled into screw orientation. The $\langle 100 \rangle$ segment is glissile on an inclined $\{110\}$ plane at 300 and 450K, and glides across the loop as the side arms cross-slip, thereby transforming the loop into a pair of superjogs, which, as in (b), becomes glissile at τ_c . The $\langle 100 \rangle$ segment is immobile at 100K, however, and the dislocation breaks away from the loop by cross-slip and mutual annihilation of its screw side arms.
- (e) τ_c lies between 290 and 160MPa for $100 \leq T \leq 450\text{K}$. These loops are stronger obstacles than voids with a similar number of vacancies because of the larger effective size of loops.
- (f) With the exception of the large loop at low temperature, the interaction process is efficient for absorption of SIA clusters from slip bands, as observed in flow localisation.

ACKNOWLEDGEMENTS

This research was sponsored by (i) grant PERFECT (F160-CT-2003-508840) under programme EURATOM FP-6 of the European Commission, (ii) a research grant from the UK Engineering and Physical Sciences Research Council and (iii) the Division of Materials Sciences and Engineering and the Office of Fusion Energy Sciences, U.S. Department of Energy, under contract DE-AC05-00OR22725 with UT-Battelle, LLC.

For Peer Review Only

References

1. D.J. Bacon, F. Gao and Yu.N. Osetsky, J. Nucl. Mater. **276** 1 (2000).
2. Yu.N. Osetsky, D.J. Bacon, A. Serra, B.N. Singh and S.I. Golubov, Phil. Mag. A **83** 61 (2003).
3. B.D. Wirth, G.R. Odette, D. Maroudas and G.E. Lucas, J. Nucl. Mater. **244** 185 (1997); *ibid.* **276** 33 (2000).
4. Yu.N. Osetsky, D.J. Bacon, A. Serra, B.N. Singh and S.I. Golubov, J. Nucl. Mater. **276** 65 (2000).
5. N. Soneda and T. Diaz de la Rubia, Phil. Mag. A **81** 331(2001).
6. B.N. Singh, A. Horsewell, P. Toft, D.J. Edwards, J. Nucl. Mater. **224** 131 (1995).
7. Yu.N. Osetsky, D.J. Bacon, F. Gao, A. Serra and B.N. Singh, J. Nucl. Mater. **283-287** 784 (2000).
8. N.M. Ghoniem, S. H. Tong, J. Huang, B.N. Singh and M. Wen, J. Nucl. Mater. **307-311** 843 (2002).
9. M. Victoria, N. Baluc, C. Bailat, Y. Dai, M.I. Luppó, R. Schaublin and B.N. Singh, J. Nucl. Mater. **276** 114 (2000).
10. B.N. Singh, H. Trinkaus and A.J.E. Foreman, J. Nucl. Mater. **249** 91 (1997); *ibid.* **251**, 172 (1997).
11. N.M. Ghoniem, S.H. Tong, B.N. Singh and L.Z. Sun, Phil. Mag. **81** 2743 (2001).
12. Z. Rong, V. Mohles, D.J. Bacon and Yu.N. Osetsky, Phil. Mag. **85** 171 (2005).
13. M.J. Makin, Phil. Mag. **10** 695 (1964).
14. B.L. Eyre and R. Bullough, Phil. Mag. **12** 31 (1965).
15. J. Marian, B.D. Wirth and J.M. Perlado, Phys. Rev. Lett. **88** 255507-1 (2002).
16. J. Marian, B.D. Wirth, R. Schäublin, G.R. Odette and J.M. Perlado, J. Nucl. Mater. **323** 181 (2003).
17. S. Jumel, J-C. Van Duysen, J. Ruste and C. Domain, J. Nucl. Mater. **346** 79 (2005).
18. Yu.N. Osetsky, D.J. Bacon, Z. Rong and B.N. Singh, Phil. Mag. Lett. **84** 745 (2004).
19. Z. Rong, Yu.N. Osetsky and D.J. Bacon, Phil. Mag. **85** 1473 (2005).
20. A. Nomoto, N. Soneda, A. Takahashi and S. Ishino, Mats. Trans. **46** 463 (2005).
21. D. Rodney and G. Martin, Phys. Rev. Lett. **82** 3273 (1999).
22. D. Rodney and G. Martin, Phys. Rev. B **71** 8714 (2000).

- 1
- 2
- 3
- 4
- 5 23. Yu.N. Osetsky and D.J. Bacon, *Modelling Simul. Mat. Sci. Eng.* **11** 427 (2003).
- 6 24. G.J. Ackland, D.J. Bacon, A.F. Calder and T. Harry, *Phil. Mag. A* **75** 713 (1997).
- 7
- 8 25. B.N. Singh, A. Horsewell and P. Toft, *J. Nucl. Mater.* **271-272** 77 (1999).
- 9
- 10 26. M.I. Luppó, C. Bailat, R. Schäublin and M. Victoria, *J. Nucl. Mater.* **283-287** 483
- 11 (2000).
- 12
- 13 27. S.J. Zinkle and B.N. Singh, *J. Nucl. Mater.* (2005), in press.
- 14
- 15 28. Yu.N. Osetsky, A. Serra and V. Priego, *J. Nucl. Mater.* **276** 202 (2000).
- 16
- 17 29. D. Hull and D.J. Bacon, *Introduction to Dislocations*, 4th edition, Butterworth-
- 18 Heinemann, 2001.
- 19
- 20 30. Yu.N. Osetsky and D.J. Bacon, *J. Nucl. Mater.* **323**, 268 (2003).
- 21
- 22 31. D.J. Bacon, Yu.N. Osetsky and Z. Rong, unpublished work.
- 23
- 24 32. F. Gao, H. Heinisch, R.J. Kurtz, Yu.N. Osetsky, R.G. Hoagland, *Phil. Mag.* **85** 619
- 25 (2005).
- 26
- 27 33. D.J. Bacon, U.F. Kocks and R.O. Scattergood, *Phil. Mag.* **26** 1242 (1973).
- 28
- 29 34. Y.N. Osetsky and D.J. Bacon, *J. Nucl. Mater.* **323** 268 (2003).
- 30
- 31 35. E. Bitzek and P. Gumbsch, *Mat. Sci. and Eng. A* **387-389** 11 (2004).
- 32
- 33
- 34
- 35
- 36
- 37
- 38
- 39
- 40
- 41
- 42
- 43
- 44
- 45
- 46
- 47
- 48
- 49
- 50
- 51
- 52
- 53
- 54
- 55
- 56
- 57
- 58
- 59
- 60

Figure captions

- Fig. 1. Schematic illustration of the edge dislocation and SIA loop in one periodic cell. The sense of positive applied stress resolved shear stress, τ , is indicated by the block arrows.
- Fig. 2. Visualisations of the spontaneous glide and absorption process of a 37-SIA loop on the edge dislocation at $T = 0\text{K}$. The value of applied strain, ϵ , corresponding to the abscissa of Fig. 3 is indicated.
- Fig. 3. τ versus ϵ plots for the glide and absorption process for a 37-SIA loop. The molecular statics (MS) simulations for $T = 0\text{K}$ are for $\Delta\epsilon$ increments of either 2 or 10×10^{-5} . The MD simulation is for $T = 100\text{K}$ and $\dot{\epsilon} = 2 \times 10^6 \text{s}^{-1}$.
- Fig. 4. τ_c versus T for 37-SIA and 331-SIA loops at various values of $\dot{\epsilon}$ in units 10^6s^{-1} . The MS ($T = 0\text{K}$) value for the small loop is the maximum on the MS plots in Fig. 3.
- Fig. 5. Visualisations of the spontaneous glide and transformation process of a 331-SIA loop at $T = 300\text{K}$ and $\dot{\epsilon} = 20 \times 10^6 \text{s}^{-1}$. The $[010]$ segment has formed in (b) and is seen to glide down as the dislocation side arms in screw orientation glide down in (c) and (d).
- Fig. 6. Schematic illustration of the processes observed in Fig. 5. The line arrows and index arrows show the positive line direction and Burgers vector as given by the RH/FS convention.
- Fig. 7. Visualisations of the interaction process for a 331-SIA loop at $T = 100\text{K}$ and $\dot{\epsilon} = 5 \times 10^6 \text{s}^{-1}$. The $[010]$ segment has formed in (a) and two dislocation side arms in screw orientation have been drawn out and started to cross-slip towards each other in (b).
- Fig. 8. τ versus ϵ plots for a 331-SIA loop at two temperatures and a 339-vacancy void for $\dot{\epsilon} = 5 \times 10^6 \text{s}^{-1}$ at $T=300\text{K}$.

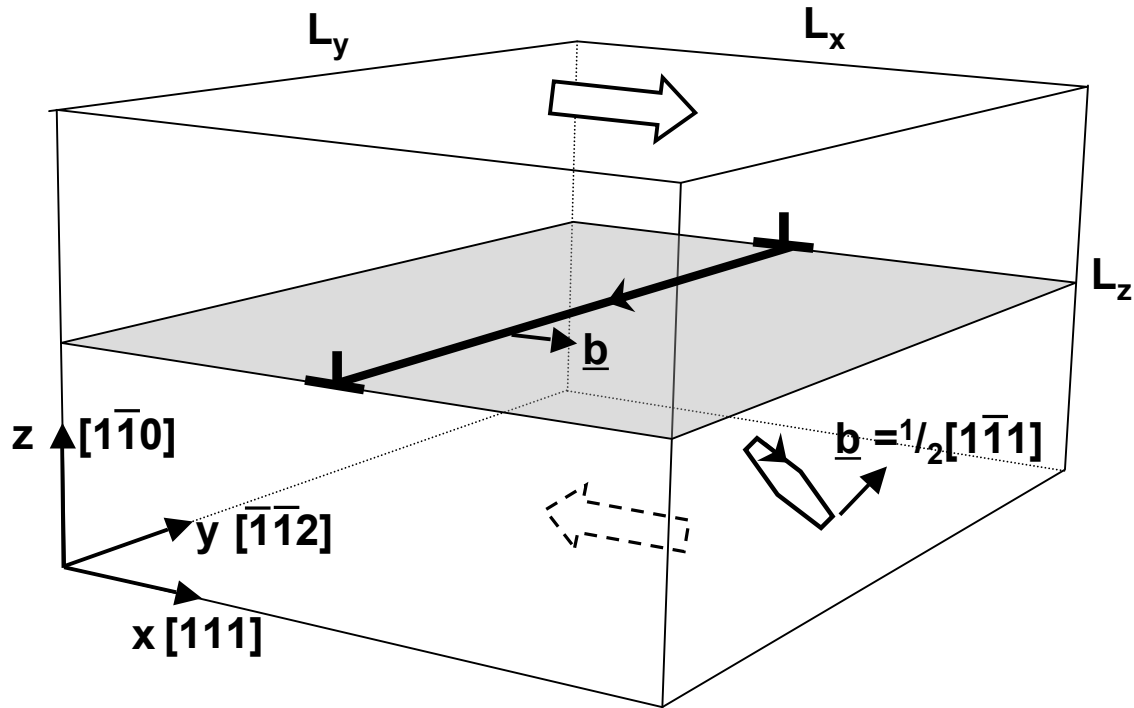


Fig. 1. Schematic illustration of the edge dislocation and SIA loop in one periodic cell. The sense of positive applied stress resolved shear stress, τ , is indicated by the block arrows.

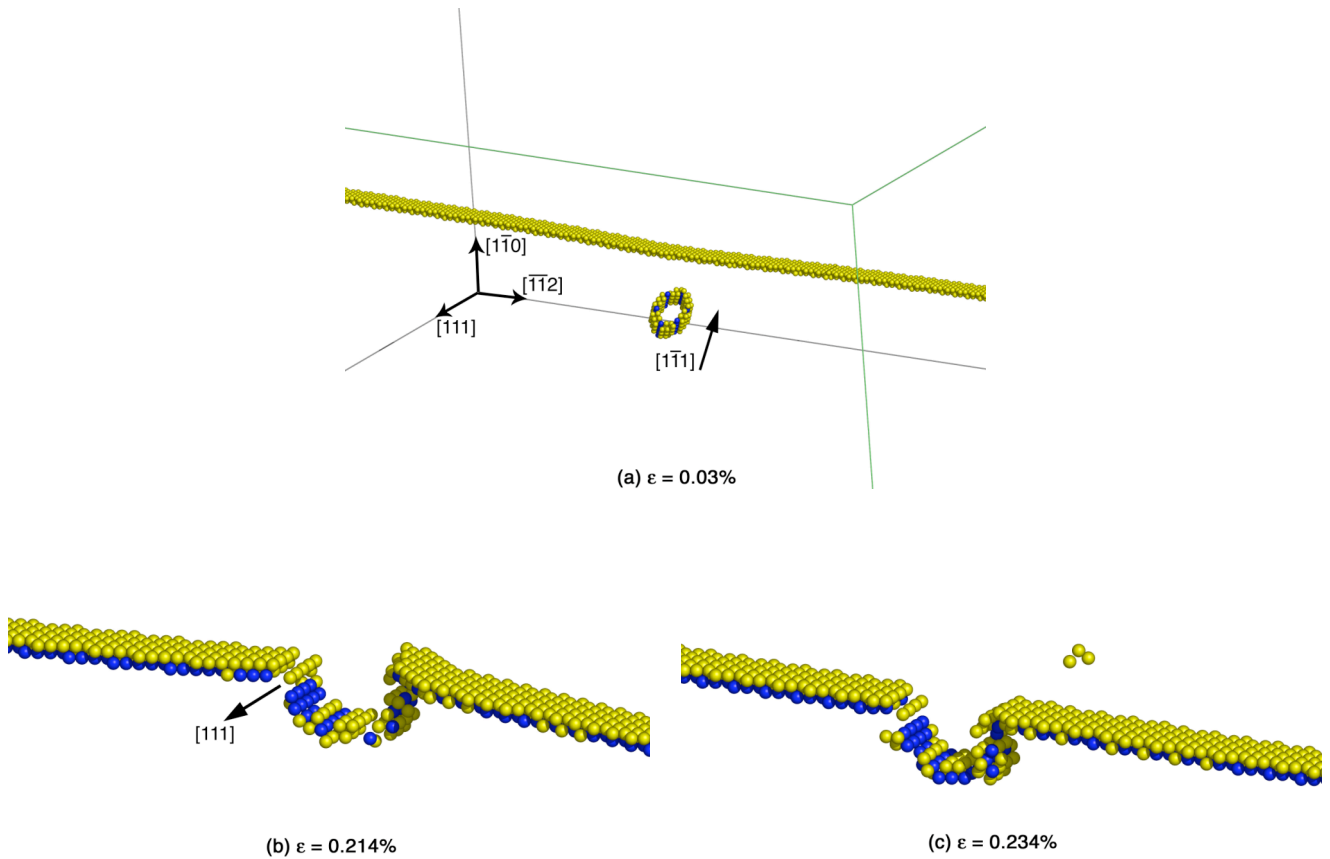


Fig. 2. Visualisations of the spontaneous glide and absorption process of a 37-SIA loop on the edge dislocation at $T = 0\text{K}$. The value of applied strain, ε , corresponding to the abscissa of Fig. 3 is indicated.

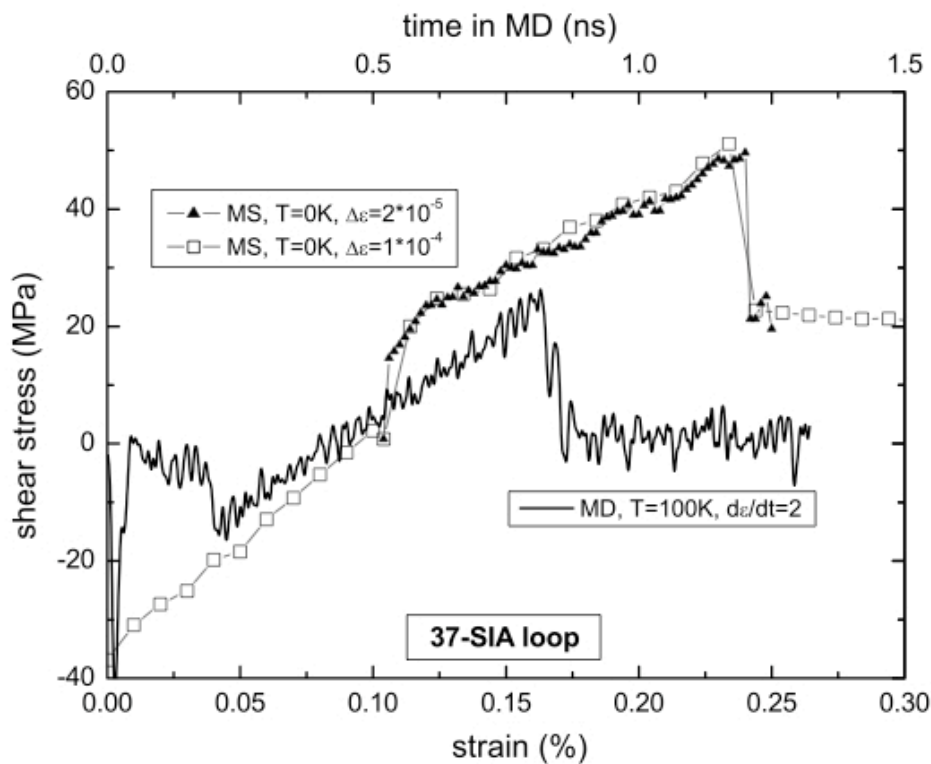


Fig. 3. τ versus ϵ plots for the glide and absorption process for a 37-SIA loop. The molecular statics (MS) simulations for $T = 0\text{K}$ are for $\Delta\epsilon$ increments of either 2×10^{-5} or 1×10^{-4} . The MD simulation is for $T = 100\text{K}$ and strain rate $= 2 \times 10^6\text{s}^{-1}$.

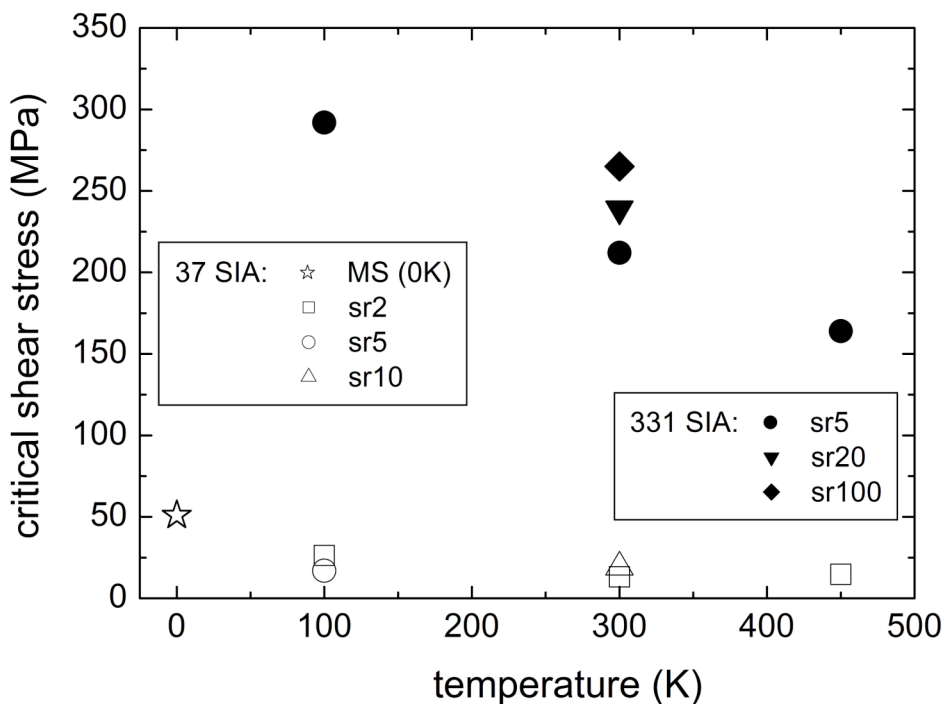


Fig. 4. τ_c versus T for 37-SIA and 331-SIA loops at various values of $\dot{\epsilon}$ in units 10^6s^{-1} . The MS ($T = 0\text{K}$) value for the small loop is the maximum on the MS plots in Fig. 3.

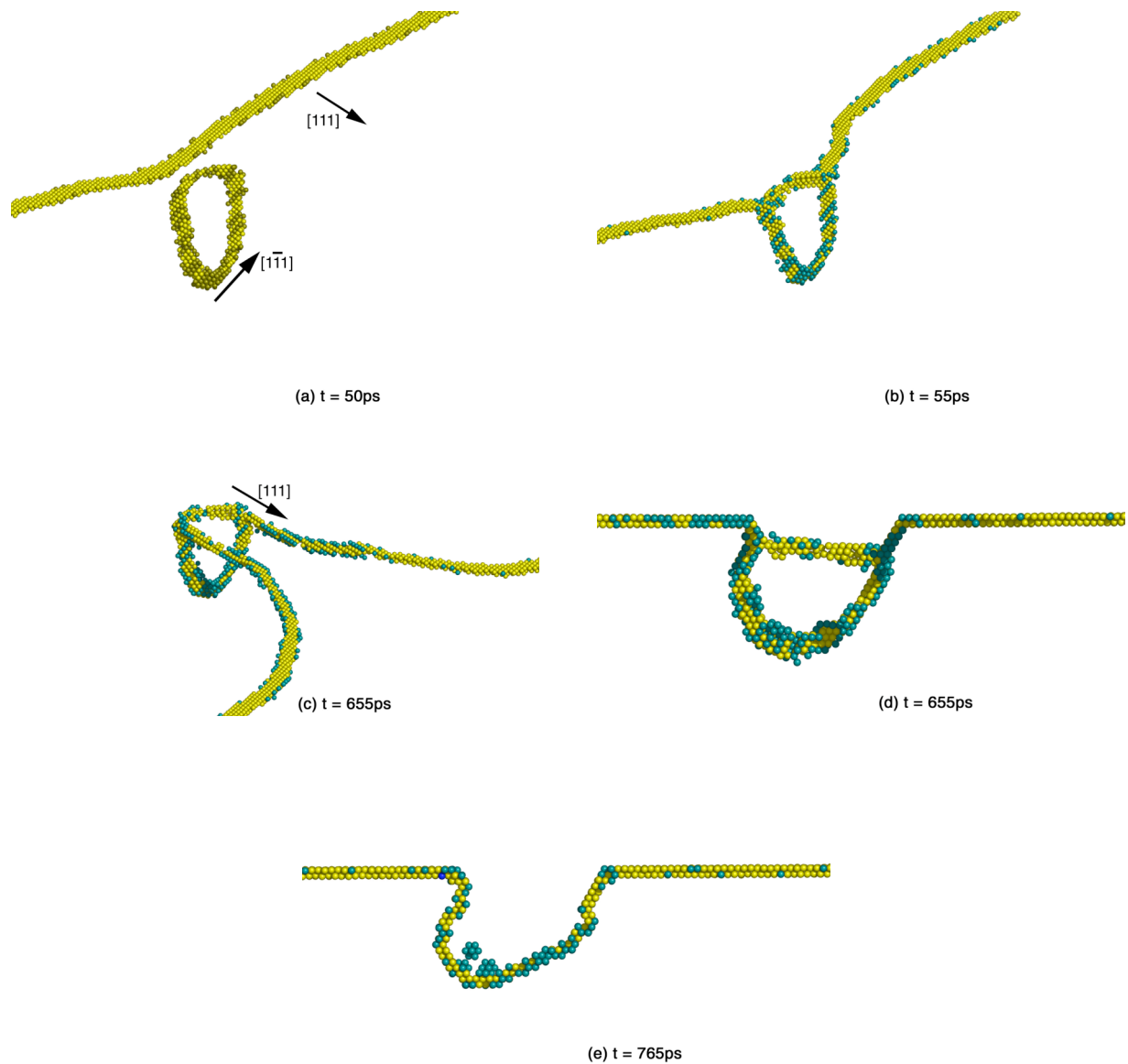


Fig. 5. Visualisations of the spontaneous glide and transformation process of a 331-SIA loop at $T = 300\text{K}$ and strain rate $= 20 \times 10^6 \text{s}^{-1}$. The $[010]$ segment has formed in (b) and is seen to glide down as the dislocation side arms in screw orientation glide down in (c) and (d).

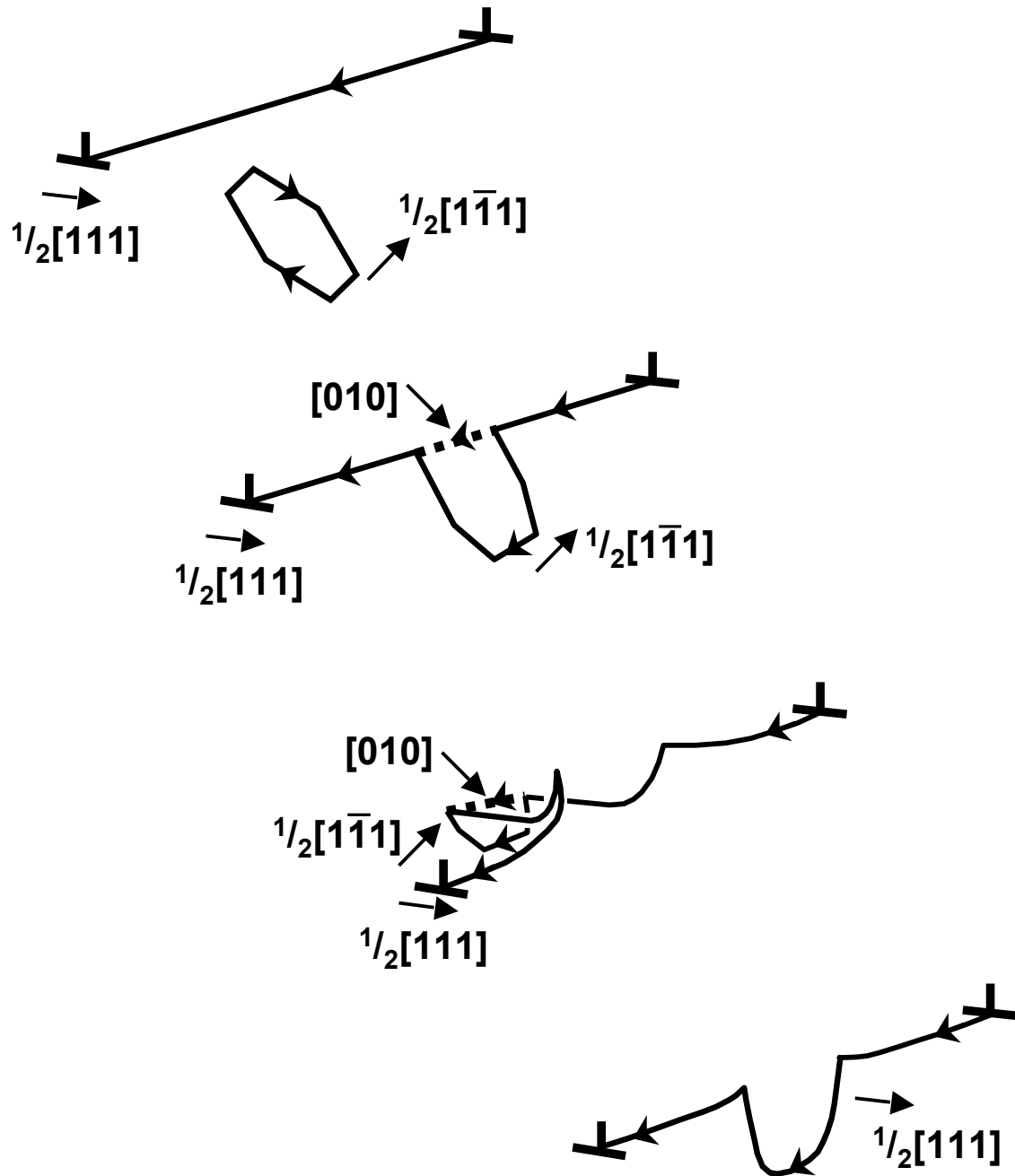
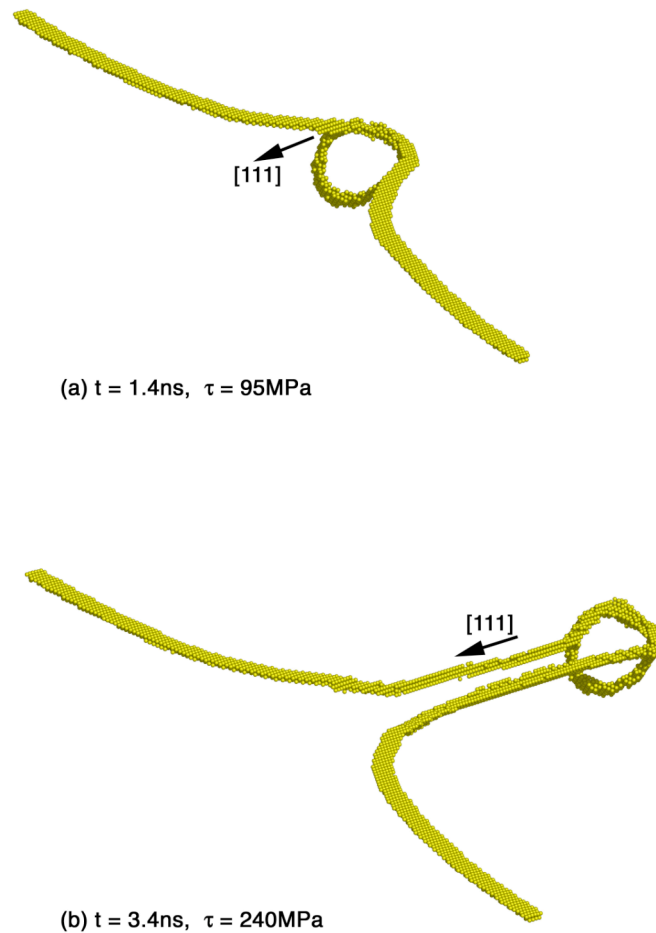


Fig. 6. Schematic illustration of the processes observed in Fig. 5. The line arrows and index arrows show the positive line direction and Burgers vector as given by the RH/FS convention.



51 Fig. 7. Visualisations of the interaction process for a 331-SIA loop at $T = 100\text{K}$ and
52 strain rate $= 5 \times 10^6 \text{s}^{-1}$. The $[010]$ segment has formed in (a) and two dislocation side arms
53 in screw orientation have been drawn out and started to cross-slip towards each other in
54 (b).
55
56
57
58
59
60

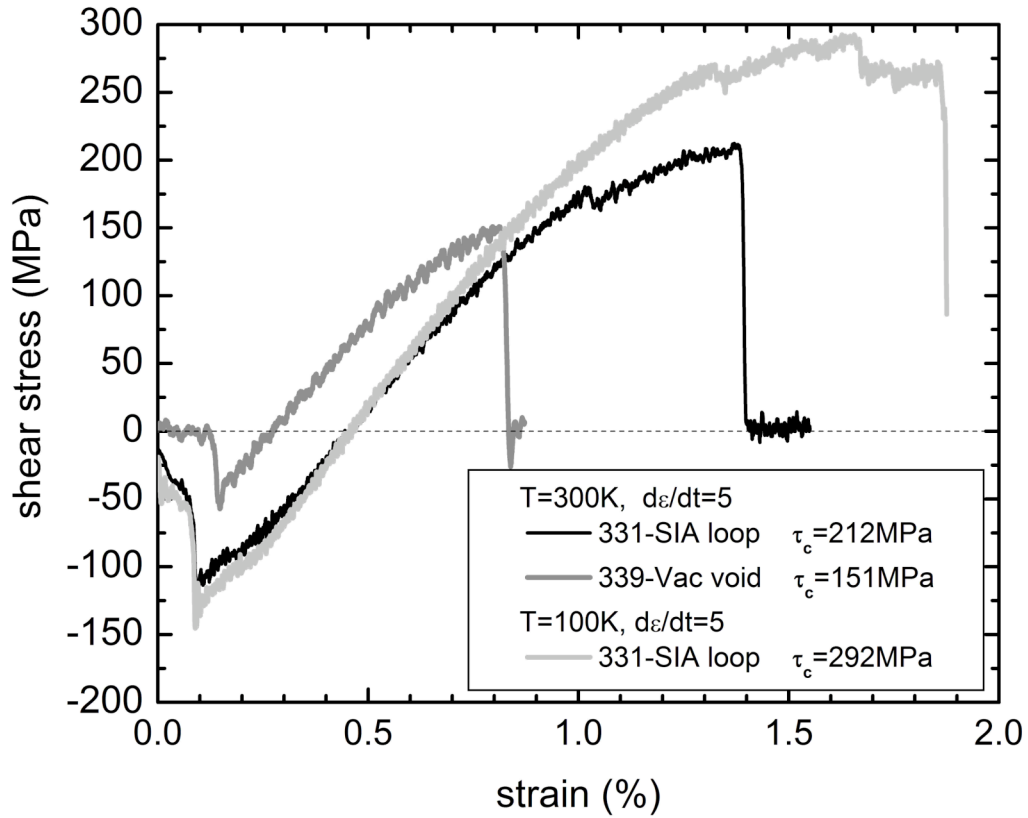


Fig.8. τ versus ε plots for a 331-SIA loop at two temperatures and a 339-vacancy void for strain rate = $5 \times 10^6 \text{s}^{-1}$ at $T=300\text{K}$.

Computer simulation of reactions between an edge dislocation and glissile self-interstitial clusters in iron

D.J. Bacon¹, Yu.N. Osetsky² and Z.Rong¹

- 1) Materials Science and Engineering, Department of Engineering, The University of Liverpool, Liverpool L69 3GH, UK.
- 2) Computer Science and Mathematics Division, Oak Ridge National Laboratory, P. O. Box 2008, Oak Ridge, TN 37831-6158, USA.

ABSTRACT

Clusters of self-interstitial atoms (SIAs) are formed in metals by high-energy displacement cascades, often in the form of small dislocation loops with a perfect Burgers vector, b . Atomic-scale computer simulation is used here to investigate their reaction with an edge dislocation gliding in α -iron under stress for the situation where b is inclined to the dislocation slip plane. b of small loops (37 SIAs here) changes spontaneously and the interstitials are absorbed as a pair of superjogs. The line glides forward at critical stress τ_c when one or more vacancies are created and the jogs adopt a glissile form. A large loop (331 SIAs here) reacts spontaneously with the dislocation to form a segment with $b = \langle 100 \rangle$, which is sessile on the dislocation slip plane, and as applied stress increases the dislocation side arms are pulled into screw orientation. At low temperature (100K), the $\langle 100 \rangle$ segment remains sessile and the dislocation eventually breaks free when the screw dipole arms cross-slip and annihilate. At 300K and above, the segment can glide across the loop and transform it into a pair of superjogs, which become glissile at τ_c . Small loops are weaker obstacles than voids with a similar number of vacancies, large loops are stronger. Irrespective of size, the interaction processes leading to superjogs are efficient for absorption of SIA clusters from slip bands, an effect observed in flow localisation.

Corresponding author: D.J. Bacon (djbacon@liv.ac.uk)

Keywords: Computer simulation, dislocation loop, interstitial cluster, iron, radiation damage

Formatted: Indent: First line: 0 pt

Formatted: Normal, Centered, Indent: First line: 18 pt, Line

Deleted: ¶

Deleted: These loops are weaker obstacles than voids with a similar number of vacancies.

Deleted: which is sessile on the dislocation slip plane but glissile on an inclined {110} plane. A

Deleted: and

Deleted: ,

Deleted: s

Deleted: s

Deleted: L

Deleted: obstacles than voids with a similar number of vacancies

Deleted: is

Deleted: ¶

Deleted: ¶

1. Introduction

Exposure of metals to fast-neutron irradiation can cause a substantial increase in yield stress and a reduction in ductility due to the interaction of dislocations with obstacles on or near their slip plane. The obstacles are formed largely by point defect clusters created in displacement cascades. Molecular dynamics (MD) computer simulations have shown that the self-interstitial atom (SIA) component of [primary](#) radiation damage is [mainly](#) in the form of platelets of closely-packed, parallel crowdions that are equivalent to small, nanometre-scale interstitial dislocation loops with perfect Burgers vector, b , parallel to the crowdion axis, [e.g.](#) [1,2]. Atomistic simulations of a variety of BCC, FCC and HCP metals have shown that such loops are glissile and move in one dimension parallel to the crowdion axis by thermally-activated events with a low activation energy of $\sim 0.02\text{eV}$ [3-5]. They have a long-range strain field and can interact with dislocations by either intersecting their slip plane or gliding to decorate them in regions where they are attracted by the dislocation stress field. The latter possibility has support from experiment, [e.g.](#) [6], and modelling, [e.g.](#) [7,8]. Further, the interaction of gliding dislocations with loops clearly influences the flow stress and ductility of irradiated metals, and is believed to play an important role in flow localisation and the formation of slip channels that appear to be cleared of radiation damage debris [9].

Decoration of dislocation sources by 'atmospheres' of interstitial loops led Singh and co-workers [10] to argue that the increase in the upper yield stress and the subsequent yield drop are related to the stress necessary to unlock dislocations from the loops that decorate them. Estimates of the unlocking stress for a straight dislocation were found to be consistent with experiment. A continuum dislocation dynamics method was later used to determine the stress for a flexible dislocation to break away from rows of loops below the slip plane and confirmed the earlier estimates [11,12]. These treatments assumed the interstitial loops to be static and unable to glide with a dislocation, whereas perfect loops are intrinsically glissile and those nearest the slip plane not only exert the largest force on the dislocation but also experience the largest force tending to make them glide. This was pointed out by Makin [13], who calculated the long-range elastic interaction between a dislocation and loop and noted that loops lying close to the glide plane of a dislocation

Deleted: (?? Refs for decoration?)

Deleted: (?? Okay? Nasr work?)

Deleted: 8

Deleted: (?? Refs for this?)

Deleted: 9,10

Deleted: 1

Deleted: 2

with the same b may be swept along with it, although the effect could not be quantified in the absence of information on the force to move a loop at the atomic scale.

The present work is part of a series of atomic-scale studies of the dynamics of dislocation behaviour in the presence of interstitial loops in α -iron (Fe). Loops with $b = \frac{1}{2}\langle 111 \rangle$ and $\langle 100 \rangle$ grow during irradiation of this metal. The origin of the latter, which have the larger elastic energy, is unclear. It has been proposed that both sets could result by shear from a common $\frac{1}{2}\langle 110 \rangle$ nucleus [14], or that two intersecting $\frac{1}{2}\langle 111 \rangle$ clusters can react to form a $\langle 100 \rangle$ loop [15]. However, neither mechanism has yet been demonstrated to occur and the $\frac{1}{2}\langle 111 \rangle$ configuration has lower energy than $\langle 100 \rangle$ using all currently available interatomic potentials. Since $\frac{1}{2}\langle 111 \rangle$ SIA clusters arise in irradiated iron and other BCC metals, we have concentrated on them in the first part of this study. In any case, it is not obvious *a priori* which creates the stronger obstacle to glide of a dislocation with $b = \frac{1}{2}\langle 111 \rangle$, because the dislocation can react favourably with a $\frac{1}{2}\langle 111 \rangle$ loop to form a $\langle 100 \rangle$ segment, which can be sessile (see later), whereas the favourable reaction with a $\langle 100 \rangle$ loop results in another $\frac{1}{2}\langle 111 \rangle$ segment, which is glissile. Thus, both loop types need to be studied and we will report on treatment of $\langle 100 \rangle$ loops in a second part.

Previously, the interaction of a $\frac{1}{2}\langle 111 \rangle\{110\}$ edge dislocation gliding under applied stress with sets of $\frac{1}{2}\langle 111 \rangle$ SIA clusters of size ~ 1 nm distributed below the extra half-plane was simulated for a range of temperature [16,17]. It was found that a row of loops can be dragged at almost the free-flight velocity of the dislocation ($\sim 100\text{ms}^{-1}$ for 10MPa at 300K). A quantitative model for this, based on a drag coefficient derived from the diffusivity of interstitial loops, was presented, and the conditions under which a dislocation breaks away from a row of glissile loops was determined. Perfect dislocation loops in this metal have b equal to one of the four possible vectors $\frac{1}{2}\langle 111 \rangle$, but only two of them are parallel to the $\{110\}$ slip plane of a dislocation and were considered for drag. Glissile loops with one of the other two b s can move to intersect the dislocation glide plane, however, and cause direct dislocation-dislocation reaction. This latter process is modelled in the present work and its dependence on temperature, T , applied shear strain rate, $\dot{\epsilon}$, and loop size analysed. We have again considered the edge dislocation.

Although it is well known that glide of screw dislocations controls slip in BCC metals at low T , it should be noted that edge dislocations have to interact/absorb/overcome loops for plastic flow to occur at any temperature. Their mechanisms therefore have to be

Deleted: glissile

Formatted: Not Highlight

Deleted:

Formatted: Not Highlight

Formatted: Font: Bold,

Formatted: Not Highlight

Formatted: Font: Italic, Not Highlight

Formatted: Not Highlight

Formatted: Font: Bold,

Formatted: Not Highlight

Formatted: Not Highlight

Formatted: Not Highlight

Deleted: Initially

Deleted: n

Deleted: in α -iron and copper

Deleted: 4

Deleted: 3

Deleted: 5

Deleted: 4

Deleted: in Fe

Deleted: The simulations concentrated on the slip system $\frac{1}{2}\langle 111 \rangle\{110\}$ in α -iron.

Deleted: ,

Deleted: and

Deleted: ,

Formatted: No underline

Formatted: No underline

investigated since there is no reason to suppose *a priori* that they are not important. Furthermore, dislocation glide can result in the production of cleared channels, as noted above, and, although some static and dynamic simulations of screw- $1/2\langle 111 \rangle$ loop interaction have been reported [18,19], we are not aware of evidence that screw dislocations absorb/remove loops to result in clear band formation.

Formatted: Font: Italic

Formatted: Not Highlight

Formatted: Not Highlight

The method employed here is summarised in section 2 and the results presented in section 3. Section 4 contains a discussion of the investigation, including an assessment of its consequences for understanding the effects of irradiation on plasticity in iron. We also compare the present results with those of a very recent MD simulation of dislocation-loop interaction in iron with the same geometry as used here by Nomoto et al. [20] and with a qualitatively similar study of dislocation-loop interaction in the FCC metal nickel by Rodney and Martin [21,22].

Deleted: 16

Deleted: 5

Deleted: 17

Deleted: 6

Deleted: ,18

Deleted: 7

Deleted: and

Deleted: ?? I haven't actually discussed Rodney and Martin in section 4 - what do you think??

Deleted: 19

Deleted: 8

2. Method and geometry

The method developed by Osetsky and Bacon [23], which treats a periodic array of edge dislocations, was employed. The x, y and z axes of the simulated crystal were oriented along [111], $[\bar{1}\bar{1}2]$ and $[1\bar{1}0]$ directions, as illustrated in Fig. 1. Periodic boundary conditions were employed in the x and y directions, corresponding to the direction of \mathbf{b} and the line direction, respectively, and fixed conditions were used across the z boundaries. Choice of crystal dimensions is important for modelling dislocation motion because the size, L_x , along the x-axis should be large enough for interactions between the dislocation and its images to be insignificant [23]. We used $L_x=120b$ (~29.8nm for Fe with model lattice parameter $a_0 = 0.2867\text{nm}$ at temperature $T = 0\text{K}$); the period, L_y , defines the inter-cluster spacing and was $59\sqrt{6}a_0$ (~41.4nm); and L_z was $49\sqrt{2}a_0$ (~19.9nm). The total number of mobile atoms in the MD cell was ~2.1M.

Deleted: 19

Deleted: 8

Rigid blocks of atoms were used at the z-axis boundaries to apply shear strain, ϵ , by displacement of the +z block. The corresponding applied shear stress, τ ($=\tau_{xz}$), was computed from the shear force on this block due to the free atoms of the inner region (see [23]). Molecular statics (MS) relaxation, i.e. potential energy minimisation, was used to simulate athermal loading at $T = 0\text{K}$ under strain increasing in increments $\Delta\epsilon = 2$ to 10×10^{-5} . Molecular dynamics (MD) with timestep 2-5fs was used for constant-strain-rate

Deleted: shear

Deleted: 18

1
2
3 deformation at $T > 0\text{K}$, with $\dot{\epsilon}$ in the range $2\text{-}100 \times 10^6 \text{s}^{-1}$ and T in the range $100\text{-}450\text{K}$, as
4 defined by the mean atomic kinetic energy. Thermal expansion was treated by changing a_0
5 until the total pressure fluctuated around zero.
6

Deleted: $\dot{\epsilon}$

7
8 The Finnis-Sinclair-type interatomic potential for Fe of Ackland et al. [24] was
9 used. The SIA clusters/loops were created in the model by inserting <111> dumbbells
10 after the dislocation had been formed and relaxed, and then relaxing the model again to
11 minimise the potential energy. They contained N interstitials and were of hexagonal shape
12 with sides of length $d = a_0(2N)^{1/2}/3$ along <112> directions. Values $N = 37$ and 331 were
13 chosen, i.e. $d = 0.82$ and 2.46nm , respectively. The centre of the cluster was positioned a
14 distance H below the slip plane, as depicted in figure 1. Values of H equal to 11 , 22 and
15 $33a_0$ were used. The two loop Burgers vectors $\frac{1}{2}[1\bar{1}1]$ and $\frac{1}{2}[\bar{1}11]$ are inclined to the
16 $(1\bar{1}0)$ slip plane, but they are symmetric with respect to the dislocation, so only one need
17 be considered. A loop with $\mathbf{b} = \frac{1}{2}[1\bar{1}1]$ is shown schematically in Fig. 1.
18
19
20
21
22
23

Deleted: 0

Deleted: 19

Deleted: by inserting <111> dumbbells

24 3. Results

25 3.1. Reaction at $T = 0\text{K}$

26
27 Under the attractive field of the dislocation, and even in the absence of thermal
28 motion of the atoms, small SIA loops glide over the H range considered to meet the
29 dislocation as it moves under strain on its slip plane. (The thickness of cleared channels
30 was not a concern of this work, but the band of interaction over which loops can glide to an
31 edge dislocation must at least $33a_0$, even at $T = 0\text{K}$. It was not feasible to model larger
32 crystals to investigate this dimension further.) The dislocation actually bows forward as a
33 loop approaches in order to assist the favourable reaction. Fig. 2(a) shows a visualisation
34 of the initial dislocation line and 37-SIA cluster viewed from the front of the model crystal
35 in Fig. 1. The dislocation has already started to bow forward slightly and as it moves
36 further under the applied strain the loop slips on its glide cylinder along $[1\bar{1}1]$ to meet it.
37 The axis of the crowdions then changes to $[111]$, i.e. \mathbf{b} of the SIA loop rotates to be the
38 same as that of the dislocation line. The newly-formed pair of superjogs restricts the slip
39 of the dislocation (Fig. 2(b)) until the SIAs that form it reorganise by self-climb and
40 emission of a vacancy in the crystal to give glissile segments on $\{110\}$ or $\{112\}$ planes of
41
42
43
44
45
46
47
48
49
50

Formatted: Not Highlight

Deleted:

Formatted: Not Highlight

Formatted: Subscript

Formatted: Not Highlight

the [111] zone axis, as seen in Fig. 2(c). The jogged dislocation then continues to glide with little hindrance.

The relationship between τ and ε during the process is plotted in Fig. 3. In the absence of any other defect, the edge dislocation glides on a {110} plane in the model at $T = 0K$ under applied resolved shear stress of about 25MPa [23]: this is the Peierls stress, τ_p . As the dislocation approaches the periodic row of SIA clusters, it is initially attracted towards them ($\tau < \tau_p$) and becomes pinned by the double superjogs formed by the reaction. τ rises as ε increases until reaching a maximum (i.e. critical) stress $\tau_c = 51MPa$, at which stage a vacancy is created and the superjogs become glissile on the $\mathbf{b} = \frac{1}{2}[111]$ system and τ falls to τ_p . The process described does not depend on the increment $\Delta\varepsilon$ used here, as seen from the two sets of data in Fig. 3.

The simulations for $T = 0K$ provide information on the equilibrium (minimum potential energy) structure at each strain increment, and the configurations are equivalent to those that would be obtained by minimising the elastic energy in the continuum approximation. However, they do not necessarily reveal information about the atomic mechanisms that would occur in a real metal where thermal effects assist the reaction process. For this reason, most modelling has been done using MD, as described in the following section.

3.2. Reaction at $T > 0K$

3.2.1. Small loops

The aim of this part of the study was to examine the effect of cluster size, temperature and $\dot{\varepsilon}$ on the reaction and strengthening mechanism. The 37-SIA cluster is considered first. Its interaction with the edge dislocation has been investigated for $T = 100, 300$ and $450K$ in a model with applied $\dot{\varepsilon}$ values in the range $2-10 \times 10^6 s^{-1}$. (For the dislocation density $(L_x L_z)^{-1}$ used here, this corresponds to dislocation velocity in steady state of $5-24 ms^{-1}$.) Under all conditions considered, the cluster glides to meet the dislocation and the axis of its crowdions rotates from $[1\bar{1}1]$ to $[111]$ when the cores of the two defects react. This results in creation of a pair of superjogs, which hinders slip of the dislocation and results in increasing τ until the interstitials in the superjogs reorganise by emitting a vacancy and form glissile segments on slip planes of the [111] zone. The

Deleted: 18

Deleted:

Deleted: T

Deleted: , however

Deleted: $\dot{\varepsilon}$ Deleted: $\dot{\varepsilon}$

before-and-after structures are the same as those for $T = 0\text{K}$ in Fig. 2. Unsurprisingly, the critical stress, τ_c , is less than at 0K . This is illustrated by the τ versus ε and time, t , plot for $T = 100\text{K}$ and $\dot{\varepsilon} = 2 \times 10^6 \text{s}^{-1}$ included in Fig. 3. The noise in the plot arises because of the non-zero temperature, but it can be seen that the dislocation, which glides at a stress of only a few MPa at this T and $\dot{\varepsilon}$, is initially attracted to the loop ($\tau < 0$), is then held back by the superjogs and eventually at $t \sim 0.8\text{ns}$ glides forward when the $\frac{1}{2}[111]$ superjogs become glissile: this final step takes place at a smaller stress (26MPa) and strain than at 0K .

The data for τ_c for the various conditions of T and $\dot{\varepsilon}$ are plotted in Fig. 4. It is seen that τ_c is almost independent of both parameters when $T > 0\text{K}$. Visualisation of the defect configuration during the loop transformation shows that rotation of b does not occur until the cores of the dislocation and loop meet. Furthermore, it is not the process that controls τ_c , for τ continues to increase beyond this rotation stage. Glide of the dislocation and absorbed loop occurs when atoms in segments of the core of the transformed loop rearrange at τ_c to form glissile superjogs.

3.2.2. Large loops

Loops containing 37 SIAs are typical of those formed directly in the primary displacement cascade process, which is consistent with the mean size $\sim 1\text{nm}$ observed experimentally at low irradiation dose ($\sim 10^{-3}\text{dpa}$) [25-27]. These loops are highly mobile and can move by mutual attraction to form larger dislocation loops, as seen in MD simulations [28] and, therefore, loop size increases with irradiation dose, reaching $\sim 5\text{nm}$ at $\sim 1\text{dpa}$ [25-27]. Thus, we now consider loops containing 331 interstitials; they have $d = 2.46\text{nm}$, which is equivalent to diameter $\sim 5\text{nm}$.

Five frames showing the interaction at 300K for $\dot{\varepsilon} = 20 \times 10^6 \text{s}^{-1}$ are presented in Fig. 5. Initially, the loop glides towards the dislocation glide plane and its upper segment attracts the dislocation, which bows forward (Fig. 5(a)). When they meet (Fig. 5(b)), the Burgers vector of the upper segment is transformed by the reaction

$$\frac{1}{2}[111] + \frac{1}{2}[\bar{1}\bar{1}\bar{1}] = [010], \quad (1)$$

which is energetically-favourable according to Frank's rule. The remainder of the initial loop retains its $\frac{1}{2}[1\bar{1}1]$ Burgers vector. The $[010]$ segment is sessile in the $(1\bar{1}0)$ slip

Deleted: eventually

Deleted: $\dot{\varepsilon}$

Deleted: Note that the qualitatively similar process was observed for a 61SIA loop of the same geometry.

Formatted: Font: Not Bold, No underline

Formatted: No underline

Deleted: ¶
What about 6li??

Formatted: Font: Not Bold

Formatted: Line spacing:

Formatted: Indent: First line: 0 pt, Line

Formatted: ... 11

Formatted: ... 21

Formatted: Font: 12 pt

Deleted: in

Deleted: cy

Deleted: 1

Deleted: 3

Deleted: :

Formatted: ... 31

Formatted: Font: 12 pt

Deleted: they

Formatted: ... 41

Formatted: Font: 12 pt

Deleted: 4

Deleted: 0

Formatted: ... 51

Formatted: Font: 12 pt

Deleted: 1

Deleted: 3

Deleted: in consistency w(... 61

Deleted: ,

Formatted: ... 71

Deleted: which

Formatted: ... 81

Formatted: Font: 12 pt

Formatted: Font: 12 pt

Formatted: ... 91

Deleted: $\dot{\varepsilon}$

Formatted: ... 101

plane of the dislocation, but glissile in the inclined (101) plane. However, it is pinned at its ends by the junctions with the $\frac{1}{2}[111]$ and $\frac{1}{2}[\bar{1}\bar{1}\bar{1}]$ lines, and is too short to bow under the applied stress. As τ increases, the $\frac{1}{2}[111]$ line segments pinned at the junctions are pulled into the screw orientation (Fig. 5(c)) and, assisted by the applied force on the [010] segment, cross-slip on $(10\bar{1})$ planes, thereby allowing the [010] segment to slip downwards on the (101) plane. This is shown in the view along $[\bar{1}\bar{1}\bar{1}]$ in Fig. 5(d). Eventually, at high enough applied stress, the downwards slip of the [010] dislocation and the [111] screw side arms completes the transformation of the loop into a pair of $\frac{1}{2}[111]$ superjogs on the gliding dislocation, wherein all 331 SIAs are contained (Fig. 5(e)). A few vacancies are formed in the crystal at the point when the dislocation glides forward at τ_c , in a similar manner to the small loop above, resulting in additional SIAs in the jogs. The reaction and transformation is completed in less than 0.8ns at this strain rate. It is shown in schematic representation in Fig. 6. The arrows denoting the direction of b are obtained using the RH/FS convention with the positive line sense indicated [29].

The maximum stress, τ_c , for the process in Fig. 5 is 220MPa and the jogged dislocation line continues to glide at $\tau = 12$ MPa. The same reaction and transformation process occurred for the other two $\dot{\epsilon}$ at 300K and at 450K. The value of τ_c depends on T and $\dot{\epsilon}$, however, as shown by the data plotted in Fig. 4. The interaction was also simulated for T = 450K and $\dot{\epsilon} = 5 \times 10^6 \text{s}^{-1}$, but with the sense of the applied strain reversed, i.e. the dislocation approached the loop from the right-hand side of the model in the schematic illustration of Fig. 1. The critical stress was the same as that in Fig. 4 and the transformation and unpinning processes were unchanged.

The interaction at 100K and $\dot{\epsilon} = 5 \times 10^6 \text{s}^{-1}$ resulted in $\tau_c = 290$ MPa (see Fig. 4) and had a different outcome. Two frames in the process are shown in Fig. 7. Creation of a [010] segment by the reaction of eq. (1) occurred again (Fig. 7(a)), but the segment was seen to be sessile in the loop plane at this low temperature and a long screw dipole formed on the $\frac{1}{2}[111]$ dislocation under increasing stress (Fig. 7(b)). The dipole eventually annihilated by cross-slip of its arms, which has started in Fig. 7(b), and the $\frac{1}{2}[1\bar{1}\bar{1}]$ loop was restored. Thus, both the strength of large loops and the ease with which they are absorbed as superjogs depend on temperature via the mobility of $\langle 100 \rangle$ segments.

4. Discussion

Deleted: the

Deleted:

Deleted: $\bar{1}\bar{1}\bar{1}$

Deleted: 5

Deleted: 1

Deleted: all

Deleted: cases of T and

Deleted: $\dot{\epsilon}$

Deleted: considered.

Deleted: $\dot{\epsilon}$

Formatted: Not Highlight

Deleted:

Deleted: The interaction was also simulated for T = 450K and $\dot{\epsilon} = 5 \times 10^6 \text{s}^{-1}$, but with the sense of the applied strain reversed, i.e. the dislocation approached the loop from the right-hand side of the model in the schematic illustration of Fig. 1. The critical stress was the same as that in Fig. 4 and the transformation and unpinning processes were unchanged.

1
2
3
4
5
6
7
8
9
10
11
12
13
14
15
16
17
18
19
20
21
22
23
24
25
26
27
28
29
30
31
32
33
34
35
36
37
38
39
40
41
42
43
44
45
46
47
48
49
50
51
52
53
54
55
56
57
58
59
60

This research shows clearly that the interaction mechanism between an edge dislocation and a $\frac{1}{2}\langle 111 \rangle$ interstitial loop whose glide cylinder intersects the dislocation slip plane depends on the size of the loop. Consequently, the obstacle strength provided by a loop against dislocation motion depends on loop size and, for large loops, also changes with temperature and applied $\underline{\epsilon}$. Small loops (37 SIAs here) offer the least resistance because, even in the absence of thermal effects ($T = 0\text{K}$), they are able to undergo rotation of the crowdion axis, \underline{b} , on meeting the dislocation and be absorbed on it as a double superjog. (A few simulations have been performed for 61-SIA loops, and the \underline{b} -rotation and loop absorption process is the same.) The maximum stress corresponds to the creation of point defects as the core of the jog segments reorganises to become glissile. The superjogs have only a small drag effect on the line after this in both statics and dynamics simulations.

Deleted: $\underline{\epsilon}$

Deleted:

This stress-assisted transformation occurs at $\tau_c = 51\text{MPa}$ at 0K and between 13 and 27MPa at $T > 0\text{K}$ when the inter-loop spacing, L_y , equals 41.4nm. This compares with $\tau_c \approx$ 100 and 118 MPa at $T = 0\text{K}$ for an edge dislocation to cut through a row of spherical voids in iron containing a similar number (27 or 59) of vacancies and with the same spacing. Thus, small dislocation loops are relatively weak obstacles compared with voids. Note, however, that all the SIAs are absorbed by the line in the form of a double superjog: only a few vacancies are absorbed by climb when a dislocation passes through a void at $T = 0\text{K}$ [30]. Furthermore, superjogs increase the interaction cross-section of a dislocation for reaction and/or annihilation with other defects in a crystal. Thus, the SIA-loop absorption process should be effective in assisting the creation of defect-free channels when slip occurs in irradiated iron.

Deleted: ??

Deleted: ??

Deleted: [??ref??].

Deleted: ?? Yuri - data for voids? ??

Deleted: 26

Deleted: 2

This absorption effect for small loops is similar to that found in simulation of edge dislocation-SIA loop interaction in nickel by Rodney and Martin [21,22]. Loops with 4-37 interstitials and a $\langle 110 \rangle$ crowdion axis were absorbed by the dislocation, which is dissociated in the FCC structure, by rotation of their axis (\underline{b}). This resulted in either transformation into a pair of superjogs on the dislocation, as here, or attachment to one of the Shockley partials by means of a dislocation junction. Furthermore, recent simulations have shown that rotation of \underline{b} also occurs for small clusters of crowdion SIAs gliding into contact with an edge dislocation of the prism-slip system in α -zirconium [31]. This metal

Deleted: 17

Deleted: 6

Deleted: 18

Deleted: 7

Deleted: double

Deleted: 2

Deleted: 7

Deleted: 6

Deleted: 3

has the HCP crystal structure, and so the rotation-absorption process requiring relatively low stress seems quite general for loops with up to a few tens of defects. Note that rotation requires contact interaction with a dislocation: it does not occur for SIA clusters in isolation if they contain more than four or five interstitials [32].

The reaction with a large loop (331 SIAs here) provides a much stronger obstacle to dislocation motion than that with a small loop because spontaneous rotation of b when the two defects first meet does not occur. Instead, a segment with $b = \langle 100 \rangle$ is formed. It is sessile in the dislocation glide plane and can only glide across the loop plane and complete the transformation to $b = \frac{1}{2}\langle 111 \rangle$ when, under sufficiently high τ , the dislocation side arms are pulled into screw orientation and then cross-slip (Fig. 6). τ_c is not only much higher but also more strongly temperature-dependent for this process. In fact, glide of the $\langle 100 \rangle$ segment does not occur at 100K, i.e. it is effectively immobile, and the high value of τ_c is controlled by cross-slip and annihilation of the arms of the $\frac{1}{2}\langle 111 \rangle$ screw dipole. In this case, the original loop is restored at dislocation breakaway, rather than absorbed.

Unlike the situation for small obstacles, τ_c for 331-SIA loops is higher than for voids with a similar number of vacancies. For example, τ_c equals 150MPa at $\dot{\epsilon} = 5 \times 10^6 \text{ s}^{-1}$ for spherical voids containing 339 vacancies in iron at 300K with the same spacing as here [30], compared with 212MPa for 331-SIA loops at 300K and 290MPa at 100K, as shown by the τ versus ϵ plots in Fig. 8. Note that the edge dislocation shape at the critical stress τ_c is similar to that in the Orowan mechanism, i.e. a dipole of two parallel screw segments with spacing close to the obstacle size. The effective size for the 331-SIA loop is larger than that for the 339-vacancy void, namely ~5nm compared with ~2nm. This is probably the main reason for the higher τ_c value for the 331-SIA loop because τ_c for the Orowan configuration scales roughly as the logarithm of the obstacle size [33].

As with small loops, all the interstitials are absorbed in the pair of glissile superjogs, except at 100K, so the process can be expected to be efficient at removing damage from slip bands. We have not investigated the size, which may be T - and $\dot{\epsilon}$ -dependent, for the transition from small-to-large loop behaviour. Extensive modelling is required and will be the subject of a later paper.

Only one line length L_w (= loop separation) is treated here, but results have general applicability for the following reasons. For large loops, where the dislocation side arms bend to the screw orientation, i.e. the line shape is that of the Orowan process (strong

Deleted: 28

Deleted: ¶

Formatted: Font: Not Bold, No underline

Deleted: ?? best ref ??

Formatted: Font: Not Bold

Deleted: and

Deleted: .

Deleted: It

Formatted: Not Highlight

Formatted: Not Highlight

Deleted: ???

Deleted: ???

Deleted: 6

Deleted: 5

Deleted: ??

Deleted: it is

Deleted: at

Deleted: $\tau - \epsilon$

Deleted: 7 [25

Deleted: 4

Deleted:]

Formatted: Subscript

Deleted: mechanism operated here

Deleted: the

Deleted: is formed at τ_c

Deleted: , ~5nm,

Deleted: reason of

Deleted: in the case of

Deleted: which

Formatted: Subscript

Deleted: 29

Deleted: 7

Deleted: 6

Deleted: ?? Yuri - data for voids? ?? In both cases the { ... [1]

Deleted: form

Deleted: a

Deleted: double

Formatted: Not Highlight

Formatted: Subscript

Formatted: Not Highlight

with other defects. This may enhance absorption of other SIAs or annihilation of vacancy defects. Investigation of this, and analysis of the drag effect such jogs have on slip, will be the subjects of a future paper.

5. Conclusions

(a) Perfect dislocation loops containing from a few tens to hundreds of self-interstitial atoms in iron lying within a few tens of nm of the slip plane of an an edge dislocation can glide to react with the dislocation when the loop Burgers vector, b , is inclined to the slip plane.

(b) The Burgers vector of small loops (37 SIAs here) changes spontaneously on contact and the interstitials are absorbed as a pair of superjogs. The line glides forward at critical stress τ_c when one or more vacancies are created and the jogs adopt glissile form.

(c) τ_c is 51 MPa at $T = 0K$ and lies between 13 and 27MPa for $100 \leq T \leq 450K$. These loops are weaker obstacles than voids with a similar number of vacancies.

(d) A large loop (331 SIAs here) reacts spontaneously with the dislocation to form a segment with $b = \langle 100 \rangle$, which is sessile on the dislocation slip plane, and as τ increases the dislocation side arms are pulled into screw orientation. The $\langle 100 \rangle$ segment is glissile on an inclined $\{110\}$ plane at 300 and 450K, and glides across the loop as the side arms cross-slip, thereby transforming the loop into a pair of superjogs, which, as in (b), becomes glissile at τ_c . The $\langle 100 \rangle$ segment is immobile at 100K, however, and the dislocation breaks away from the loop by cross-slip and mutual annihilation of its screw side arms.

(e) τ_c lies between 290 and 160MPa for $100 \leq T \leq 450K$. These loops are stronger obstacles than voids with a similar number of vacancies because of the larger effective size of loops.

(f) With the exception of the large loop at low temperature, the interaction process is efficient for absorption of SIA clusters from slip bands, as observed in flow localisation.

Deleted: a

Formatted: Bullets and Numbering

Deleted: but

Deleted: . As τ increases and the dislocation side arms are pulled into screw orientation, the segment

Deleted: and

Deleted: s it

Deleted: 250(

Deleted: ??

Deleted: ? - not finished yet. Current stress is ~200 at $\epsilon \sim 1$?)

Deleted: Irrespective of size

Deleted: n.

ACKNOWLEDGEMENTS

This research was sponsored by (i) grant PERFECT (F160-CT-2003-508840) under programme EURATOM FP-6 of the European Commission, (ii) a research grant from the UK Engineering and Physical Sciences Research Council and (iii) the Division of Materials Sciences and Engineering and the Office of Fusion Energy Sciences, U.S. Department of Energy, under contract DE-AC05-00OR22725 with UT-Battelle, LLC.

For Peer Review Only

References

1. D.J. Bacon, F. Gao and Yu.N. Osetsky, J. Nucl. Mater. **276** 1 (2000).
2. Yu.N. Osetsky, D.J. Bacon, A. Serra, B.N. Singh and S.I. Golubov, Phil. Mag. A **83** 61 (2003).
3. B.D. Wirth, G.R. Odette, D. Maroudas and G.E. Lucas, J. Nucl. Mater. **244** 185 (1997); *ibid.* **276** 33 (2000).
4. Yu.N. Osetsky, D.J. Bacon, A. Serra, B.N. Singh and S.I. Golubov, J. Nucl. Mater. **276** 65 (2000).
5. N. Soneda and T. Diaz de la Rubia, Phil. Mag. A **81** 331(2001).
6. B.N. Singh, A. Horsewell, P. Toft, D.J. Edwards, J. Nucl. Mater. **224** 131 (1995).
7. Yu.N. Osetsky, D.J. Bacon, F. Gao, A. Serra and B.N. Singh, J. Nucl. Mater. **283-287** 784 (2000).
8. N.M. Ghoniem, S. H. Tong, J. Huang, B.N. Singh and M. Wen, J. Nucl. Mater. **307-311** 843 (2002).
9. M. Victoria, N. Baluc, C. Bailat, Y. Dai, M.I. Luppo, R. Schaublin and B.N. Singh, J. Nucl. Mater. **276** 114 (2000).
10. B.N. Singh, H. Trinkaus, and A.J.E. Foreman, J. Nucl. Mater. **249** 91 (1997); *ibid.* **251**, 172 (1997).
11. N.M. Ghoniem, S.H. Tong, B.N. Singh and L.Z. Sun, Phil. Mag. **81** 2743 (2001).
12. Z. Rong, V. Mohles, D.J. Bacon and Yu.N. Osetsky, Phil. Mag. **85** 171 (2005).
13. M.J. Makin, Phil. Mag. **10** 695 (1964).
14. B.L. Eyre and R. Bullough, Phil. Mag. **12** 31 (1965).
15. J. Marian, B.D. Wirth and J.M. Perlado, Phys. Rev. Lett. **88** 255507-1 (2002).
16. J. Marian, B.D. Wirth, R. Schäublin, G.R. Odette and J.M. Perlado, J. Nucl. Mater. **323** 181 (2003).
17. S. Jumel, J-C. Van Duysen, J Ruste and C. Domain, J. Nucl. Mater. **346** 79 (2005).
18. Yu.N. Osetsky, D.J. Bacon, Z. Rong and B.N. Singh, Phil. Mag. Lett. **84** 745 (2004).
19. Z. Rong, Yu.N. Osetsky and D.J. Bacon, Phil. Mag. **85** 1473 (2005).
20. A. Nomoto, N. Soneda, A. Takahashi and S. Ishino, Mats. Trans. **46** 463 (2005).
21. D. Rodney and G. Martin, Phys. Rev. Lett. **82** 3273 (1999).
22. D. Rodney and G. Martin, Phys. Rev. B **71** 8714 (2000).

Formatted: Bullets and Numbering

Deleted: ¶

Formatted: English U.K.

Formatted: ... [26]

Deleted: N.

Formatted: ... [27]

Deleted: ¶

Formatted: Bullets and Numbering ... [28]

Formatted: ... [29]

Deleted: ¶

Formatted: Font: Not Bold

Formatted: ... [20]

Formatted: ... [21]

Formatted: Bullets and Numbering ... [22]

Deleted: ... [23]

Formatted: ... [24]

Formatted: ... [25]

Formatted: ... [26]

Formatted: ... [27]

Deleted: ?

Formatted: ... [28]

Deleted: ,

Formatted: ... [29]

Deleted: ,

Formatted: ... [30]

Deleted: <#>B.N. Singh, ... [31]

Formatted: Bullets and Numbering ... [32]

Formatted: ... [33]

Formatted: Dutch Belgium

Deleted: os

Formatted: ... [34]

Formatted: Bullets and Numbering ... [35]

Formatted: ... [36]

Formatted: ... [37]

Formatted: Bullets and Numbering ... [38]

23. Yu.N. Osetsky and D.J. Bacon, *Modelling Simul. Mat. Sci. Eng.* **11** 427 (2003).

24. G.J. Ackland, D.J. Bacon, A.F. Calder and T. Harry, *Phil. Mag. A* **75** 713 (1997).

25. [B.N. Singh, A. Horsewell and P. Toft, *J. Nucl. Mater.* **271-272** 77 \(1999\).](#)

26. [M.I. Lупpo, C. Bailat, R. Schäublin and M. Victoria, *J. Nucl. Mater.* **283-287** 483 \(2000\).](#)

27. [S.J. Zinkle and B.N. Singh, *J. Nucl. Mater.* \(2005\), in press.](#)

28. Yu.N. Osetsky, A. Serra and V. Priego, *J. Nucl. Mater.* **276** 202 (2000).

29. D. Hull and D.J. Bacon, *Introduction to Dislocations*, 4th edition, Butterworth-Heinemann, 2001.

30. Yu.N. Osetsky and D.J. Bacon, *J. Nucl. Mater.* **323**, 268 (2003).

31. D.J. Bacon, Yu.N. Osetsky and Z. Rong, unpublished work.

32. [F. Gao, H. Heinisch, R.J. Kurtz, Yu.N. Osetsky, R.G. Hoagland, *Phil. Mag.* **85** 619 \(2005\).](#)

33. D.J. Bacon, U.F. Kocks and R.O. Scattergood, *Phil Mag.* **26** 1242 (1973).

34. Yu.N. Osetsky and D.J. Bacon, *J. Nucl. Mater.* **323** 268 (2003).

35. E. Bitzek and P. Gumbsch, *Mat. Sci. and Eng. A* **387-389** 11 (2004).

Deleted: , [39]

Formatted ... [40]

Formatted ... [41]

Deleted: d [42]

Formatted ... [43]

Deleted: , [44]

Formatted ... [45]

Formatted ... [46]

Deleted: , [47]

Deleted: ?? Ref? [48]

Formatted ... [49]

Formatted ... [50]

Deleted: d [51]

Formatted ... [52]

Formatted ... [53]

Formatted ... [54]

Formatted ... [55]

Formatted ... [56]

Formatted ... [57]

Formatted: Bullets and Numbering ... [58]

Formatted: Bullets and Numbering ... [59]

Formatted ... [60]

Formatted: Bullets and Numbering ... [61]

Formatted ... [62]

Formatted ... [63]

Formatted ... [64]

Formatted ... [65]

Formatted ... [66]

Formatted ... [67]

Deleted: os [68]

Formatted ... [69]

Deleted: , [70]

Deleted: , [71]

Deleted: , [72]

Deleted: <#>D.J. Bacon, ... [73]

Formatted ... [74]

Figure captions

Fig. 1. Schematic illustration of the edge dislocation and SIA loop in one periodic cell.

The sense of positive applied stress resolved shear stress, τ , is indicated by the block arrows.

Fig. 2. Visualisations of the spontaneous glide and absorption process of a 37-SIA loop on the edge dislocation at $T = 0\text{K}$. The value of applied strain, ϵ , corresponding to the abscissa of Fig. 3 is indicated.

Fig. 3. τ versus ϵ plots for the glide and absorption process for a 37-SIA loop. The molecular statics (MS) simulations for $T = 0\text{K}$ are for $\Delta\epsilon$ increments of either 2 or 10×10^{-5} . The MD simulation is for $T = 100\text{K}$ and $\dot{\epsilon} = 2 \times 10^6 \text{s}^{-1}$.

Fig. 4. τ_c versus T for 37-SIA and 331-SIA loops at various values of $\dot{\epsilon}$ in units 10^6s^{-1} . The MS ($T = 0\text{K}$) value for the small loop is the maximum on the MS plots in Fig. 3.

Fig. 5. Visualisations of the spontaneous glide and transformation process of a 331-SIA loop at $T = 300\text{K}$ and $\dot{\epsilon} = 20 \times 10^6 \text{s}^{-1}$. The [010] segment has formed in (b) and is seen to glide down as the dislocation side arms in screw orientation glide down in (c) and (d).

Fig. 6. Schematic illustration of the processes observed in Fig. 5. The line arrows and index arrows show the positive line direction and Burgers vector as given by the RH/FS convention.

Fig. 7. Visualisations of the interaction process for a 331-SIA loop at $T = 100\text{K}$ and $\dot{\epsilon} = 5 \times 10^6 \text{s}^{-1}$. The [010] segment has formed in (a) and two dislocation side arms in screw orientation have been drawn out and started to cross-slip towards each other in (b).

Fig. 8. τ versus ϵ plots for a 331-SIA loop at two temperatures and a 339-vacancy void for $\dot{\epsilon} = 5 \times 10^6 \text{s}^{-1}$ at $T = 300\text{K}$.

Formatted: Justified,
Line spacing: 1.5 lines

Deleted: for

Deleted: ϵ

Formatted: Line spacing:
1.5 lines

Deleted: 5

Formatted: Not Highlight

Formatted: Not Highlight

Field Code Changed

Formatted: Line spacing:
1.5 lines

Deleted: 7

Deleted: c

Deleted: T

Deleted: r

Deleted: $\dot{\epsilon}$

Formatted: Font: 12 pt,
Complex Script Font: 12

Deleted: ¶

Formatted: Font: 12 pt,
Complex Script Font: 12

Deleted: ¶

¶

¶

¶

¶

¶

¶

¶

¶

Formatted: Justified,
Indent: Before: 0 pt,
Hanging: 42.55 pt, Line
spacing: 1.5 lines

1
2
3 Page 6: [1] Formatted David Bacon 1/10/2006 1:27:00 PM
4 Font: 12 pt, Complex Script Font: 12 pt

5 Page 6: [2] Formatted David Bacon 10/4/2005 1:51:00 PM
6 Normal, Justified, Tabs: 35.45 pt, Left

7 Page 6: [3] Formatted David Bacon 1/10/2006 1:27:00 PM
8 Font: 12 pt, Complex Script Font: 12 pt

9 Page 6: [4] Formatted David Bacon 1/10/2006 1:27:00 PM
10 Font: 12 pt, Complex Script Font: 12 pt

11 Page 6: [5] Formatted David Bacon 1/10/2006 1:27:00 PM
12 Font: 12 pt, Complex Script Font: 12 pt

13 Page 6: [6] Deleted OSETSKIYYNXPLAP 10/12/2005 12:06:00 AM
14 in consistency with loop sizes observed experimentally [??ref?].

15 Page 6: [7] Formatted David Bacon 1/10/2006 1:27:00 PM
16 Font: 12 pt, Complex Script Font: 12 pt

17 Page 6: [8] Formatted David Bacon 1/10/2006 1:27:00 PM
18 Font: 12 pt, Complex Script Font: 12 pt

19 Page 6: [9] Formatted David Bacon 1/10/2006 1:27:00 PM
20 Font: 12 pt, Complex Script Font: 12 pt

21 Page 6: [10] Formatted David Bacon 1/10/2006 1:27:00 PM
22 Font: 12 pt, Complex Script Font: 12 pt

23 Page 9: [11] Deleted OSETSKIYYNXPLAP 10/12/2005 12:23:00 AM
24 **?? Yuri - data for voids? ??** In both cases the screw dipole configuration is

25 achieved at τ_c , but the size, i.e. diameter, is larger for a loop and so τ_c , which scales
26 roughly as the logarithm of size for voids and, presumably loops, is also larger

27 Page 10: [12] Formatted David Bacon 1/10/2006 1:27:00 PM
28 Subscript, Not Highlight

29 Page 10: [13] Formatted David Bacon 1/10/2006 1:27:00 PM
30 Subscript, Not Highlight

31 Page 10: [14] Formatted David Bacon 1/10/2006 1:27:00 PM
32 Superscript, Not Highlight

33 Page 10: [15] Formatted David Bacon 1/10/2006 1:27:00 PM
34 Subscript, Not Highlight

35 Page 13: [16] Formatted OSETSKIYYNXPLAP 10/3/2005 1:04:00 AM
36 Indent: Before: 0 pt, Hanging: 27 pt, After: 0 pt, Numbered + Level: 1 + Numbering Style: 1, 2, 3, ... +
37 Start at: 1 + Alignment: Left + Aligned at: 18 pt + Tab after: 36 pt + Indent at: 36 pt, Tabs: Not at 36 pt +
38 453.6 pt

39 Page 13: [17] Formatted David Bacon 1/10/2006 1:27:00 PM
40 Spanish Spain-Modern Sort

41 Page 13: [18] Change OSETSKIYYNXPLAP 10/3/2005 1:24:00 AM
42 Formatted Bullets and Numbering

43 Page 13: [19] Formatted David Bacon 1/10/2006 1:27:00 PM
44 Font: (Default) Times New Roman, 12 pt, Complex Script Font: Times New Roman, 12 pt

45 Page 13: [19] Formatted David Bacon 1/10/2006 1:27:00 PM
46 Font: (Default) Times New Roman, 12 pt, Complex Script Font: Times New Roman, 12 pt

1			
2			
3	Page 13: [19] Formatted	David Bacon	1/10/2006 1:27:00 PM
4	Font: (Default) Times New Roman, 12 pt, Bold, Complex Script Font: Times New Roman, 12 pt		
5	Page 13: [19] Formatted	David Bacon	1/10/2006 1:27:00 PM
6	Font: (Default) Times New Roman, 12 pt, Complex Script Font: Times New Roman, 12 pt		
7			
8	Page 13: [19] Formatted	David Bacon	1/10/2006 1:27:00 PM
9	Font: Not Bold		
10	Page 13: [19] Formatted	David Bacon	1/10/2006 1:27:00 PM
11	Font: (Default) Times New Roman, 12 pt, Complex Script Font: Times New Roman, 12 pt		
12	Page 13: [20] Formatted	OSETSKIYYNXPLAP	10/3/2005 1:24:00 AM
13	Indent: Before: 0 pt, Hanging: 27 pt, Line spacing: 1.5 lines, Numbered + Level: 1 + Numbering Style: 1, 2, 3, ... + Start at: 1 + Alignment: Left + Aligned at: 18 pt + Tab after: 36 pt + Indent at: 36 pt, Tabs: Not at 18 pt + 36 pt		
14	Page 13: [21] Formatted	David Bacon	1/10/2006 1:27:00 PM
15	Font: 12 pt, Complex Script Font: 12 pt		
16	Page 13: [22] Change	OSETSKIYYNXPLAP	10/13/2005 12:07:00 AM
17	Formatted Bullets and Numbering		
18	Page 13: [23] Deleted	David Bacon	10/12/2005 7:43:00 PM
19			
20	Page 13: [23] Deleted	David Bacon	10/12/2005 7:43:00 PM
21			
22			
23			
24			
25	Page 13: [24] Formatted	David Bacon	1/10/2006 1:27:00 PM
26	Font: 12 pt, Complex Script Font: 12 pt		
27	Page 13: [24] Formatted	David Bacon	1/10/2006 1:27:00 PM
28	Font: 12 pt, Complex Script Font: 12 pt		
29	Page 13: [24] Formatted	David Bacon	1/10/2006 1:27:00 PM
30	English U.S.		
31	Page 13: [25] Formatted	David Bacon	1/10/2006 1:27:00 PM
32	Font: (Default) Times New Roman, 12 pt, Complex Script Font: Times New Roman, 12 pt		
33	Page 13: [26] Formatted	OSETSKIYYNXPLAP	10/3/2005 1:24:00 AM
34	Indent: Before: 0 pt, Hanging: 27 pt, Line spacing: 1.5 lines, Numbered + Level: 1 + Numbering Style: 1, 2, 3, ... + Start at: 1 + Alignment: Left + Aligned at: 18 pt + Tab after: 36 pt + Indent at: 36 pt, Tabs: Not at 18 pt + 36 pt		
35	Page 13: [27] Formatted	David Bacon	1/10/2006 1:27:00 PM
36	Font: (Default) Times New Roman, 12 pt, Complex Script Font: Times New Roman, 12 pt		
37	Page 13: [27] Formatted	David Bacon	1/10/2006 1:27:00 PM
38	Font: (Default) Times New Roman, 12 pt, Complex Script Font: Times New Roman, 12 pt		
39	Page 13: [28] Formatted	David Bacon	1/10/2006 1:27:00 PM
40	Font: (Default) Times New Roman, 12 pt, Complex Script Font: Times New Roman, 12 pt		
41	Page 13: [28] Formatted	David Bacon	1/10/2006 1:27:00 PM
42	Font: (Default) Times New Roman, 12 pt, Complex Script Font: Times New Roman, 12 pt		
43	Page 13: [28] Formatted	David Bacon	1/10/2006 1:27:00 PM
44	Font: (Default) Times New Roman, 12 pt, Complex Script Font: Times New Roman, 12 pt		
45	Page 13: [28] Formatted	David Bacon	1/10/2006 1:27:00 PM
46	Font: (Default) Times New Roman, 12 pt, Complex Script Font: Times New Roman, 12 pt		
47	Page 13: [28] Formatted	David Bacon	1/10/2006 1:27:00 PM
48	Font: (Default) Times New Roman, 12 pt, Complex Script Font: Times New Roman, 12 pt		
49	Page 13: [28] Formatted	David Bacon	1/10/2006 1:27:00 PM
50	Font: (Default) Times New Roman, 12 pt, Complex Script Font: Times New Roman, 12 pt		
51	Page 13: [28] Formatted	David Bacon	1/10/2006 1:27:00 PM
52	Font: (Default) Times New Roman, 12 pt, Complex Script Font: Times New Roman, 12 pt		
53	Page 13: [28] Formatted	David Bacon	1/10/2006 1:27:00 PM
54	Font: (Default) Times New Roman, 12 pt, Complex Script Font: Times New Roman, 12 pt		
55	Page 13: [28] Formatted	David Bacon	1/10/2006 1:27:00 PM
56	Font: (Default) Times New Roman, 12 pt, Not Italic, Complex Script Font: Times New Roman, 12 pt		
57	Page 13: [28] Formatted	David Bacon	1/10/2006 1:27:00 PM
58	Font: (Default) Times New Roman, 12 pt, Not Italic, Complex Script Font: Times New Roman, 12 pt		
59			
60			

1			
2			
3			
4	Page 13: [29] Formatted	David Bacon	1/10/2006 1:27:00 PM
5	Font: (Default) Times New Roman, 12 pt, Complex Script Font: Times New Roman, 12 pt		
6	Page 13: [30] Formatted	David Bacon	1/10/2006 1:27:00 PM
7	Font: (Default) Times New Roman, 12 pt, Complex Script Font: Times New Roman, 12 pt		
8	Page 13: [30] Formatted	David Bacon	1/10/2006 1:27:00 PM
9	Font: (Default) Times New Roman, 12 pt, Complex Script Font: Times New Roman, 12 pt		
10	Page 13: [30] Formatted	David Bacon	1/10/2006 1:27:00 PM
11	Font: (Default) Times New Roman, 12 pt, Complex Script Font: Times New Roman, 12 pt		
12	Page 13: [30] Formatted	David Bacon	1/10/2006 1:27:00 PM
13	English U.S.		
14	Page 13: [31] Deleted	OSETSKIYYNXPLAP	10/3/2005 1:30:00 AM
15	B.N. Singh, A.J.E. Foreman and H. Trinkaus, J. Nucl. Mater. 249 103(1997).		
16	H. Trinkaus, B.N. Singh and A.J.E. Foreman, J. Nucl. Mater. 249 91 (1997).		
17			
18			
19			
20	Page 13: [32] Change	OSETSKIYYNXPLAP	10/11/2005 11:45:00 PM
21	Formatted Bullets and Numbering		
22	Page 13: [33] Formatted	David Bacon	1/10/2006 1:27:00 PM
23	Font: Not Bold		
24	Page 13: [34] Formatted	David Bacon	1/10/2006 1:27:00 PM
25	Font: 12 pt, Not Italic		
26	Page 13: [34] Formatted	David Bacon	1/10/2006 1:27:00 PM
27	Font: 12 pt, Not Italic		
28	Page 13: [34] Formatted	David Bacon	1/10/2006 1:27:00 PM
29	Font: 12 pt, Not Italic		
30	Page 13: [34] Formatted	David Bacon	1/10/2006 1:27:00 PM
31	Font: 12 pt, Not Italic		
32	Page 13: [34] Formatted	David Bacon	1/10/2006 1:27:00 PM
33	Font: 12 pt, Bold, Not Italic		
34	Page 13: [34] Formatted	David Bacon	1/10/2006 1:27:00 PM
35	Font: 12 pt, Not Italic		
36	Page 13: [34] Formatted	David Bacon	1/10/2006 1:27:00 PM
37	Font: 12 pt, Not Italic		
38	Page 13: [34] Formatted	David Bacon	1/10/2006 1:27:00 PM
39	Font color: Auto, Dutch Belgium		
40	Page 13: [35] Change	David Bacon	12/4/2005 7:51:00 PM
41	Formatted Bullets and Numbering		
42	Page 13: [36] Formatted	David Bacon	1/10/2006 1:27:00 PM
43	Font: Bold		
44	Page 13: [36] Formatted	David Bacon	1/10/2006 1:27:00 PM
45	Font: 12 pt		
46	Page 13: [36] Formatted	David Bacon	1/10/2006 1:27:00 PM
47	Font: Times New Roman, Dutch Belgium		
48	Page 13: [37] Formatted	David Bacon	1/10/2006 1:27:00 PM
49	Font: Bold		
50	Page 13: [37] Formatted	David Bacon	1/10/2006 1:27:00 PM
51	Dutch Belgium		
52	Page 13: [38] Change	OSETSKIYYNXPLAP	10/11/2005 11:45:00 PM
53	Formatted Bullets and Numbering		
54			
55			
56			
57			
58			
59			
60			

1			
2			
3	Page 14: [39] Formatted	David Bacon	1/10/2006 1:27:00 PM
4	Font: 12 pt, Complex Script Font: 12 pt		
5	Page 14: [40] Formatted	David Bacon	1/10/2006 1:27:00 PM
6	Font: 12 pt, Complex Script Font: 12 pt		
7	Page 14: [41] Formatted	David Bacon	1/10/2006 1:27:00 PM
8	Font: 12 pt, Complex Script Font: 12 pt		
9	Page 14: [42] Formatted	David Bacon	1/10/2006 1:27:00 PM
10	Font: 12 pt, Complex Script Font: 12 pt		
11	Page 14: [43] Formatted	David Bacon	1/10/2006 1:27:00 PM
12	Font: 12 pt, Bold, No underline, Complex Script Font: 12 pt		
13	Page 14: [44] Formatted	David Bacon	1/10/2006 1:27:00 PM
14	Font: 12 pt, Bold, Complex Script Font: 12 pt		
15	Page 14: [45] Formatted	David Bacon	1/10/2006 1:27:00 PM
16	Font: 12 pt, Bold, No underline, Complex Script Font: 12 pt		
17	Page 14: [46] Formatted	David Bacon	1/10/2006 1:27:00 PM
18	Font: 12 pt, Complex Script Font: 12 pt		
19	Page 14: [47] Deleted	David Bacon	10/12/2005 7:44:00 PM
20			
21			
22			
23			
24			
25	M.I. Luppó, C. Bailat, R. Schäublin and M. Victoria, J.Nucl. Mater., 283-287 483 (2000).		
26			
27	Page 14: [48] Formatted	David Bacon	1/10/2006 1:27:00 PM
28	Font: 12 pt, Complex Script Font: 12 pt		
29	Page 14: [49] Formatted	David Bacon	1/10/2006 1:27:00 PM
30	Font: 12 pt, Not Bold, No underline, Complex Script Font: 12 pt		
31	Page 14: [50] Formatted	David Bacon	10/12/2005 7:44:00 PM
32	Indent: Before: 0 pt, Hanging: 28.35 pt, Numbered + Level: 1 + Numbering Style: 1, 2, 3, ... + Start at: 1 + Alignment: Left + Aligned at: 18 pt + Tab after: 36 pt + Indent at: 36 pt, Tabs: 28.35 pt, List tab + Not at 36 pt		
33	Page 14: [51] Formatted	David Bacon	1/10/2006 1:27:00 PM
34	Font: 12 pt, Complex Script Font: 12 pt		
35	Page 14: [52] Formatted	David Bacon	1/10/2006 1:27:00 PM
36	Font: 12 pt, Complex Script Font: 12 pt		
37	Page 14: [53] Formatted	David Bacon	1/10/2006 1:27:00 PM
38	Font: 12 pt, Bold, No underline, Complex Script Font: 12 pt		
39	Page 14: [54] Formatted	David Bacon	1/10/2006 1:27:00 PM
40	Font: 12 pt, Bold, Complex Script Font: 12 pt		
41	Page 14: [55] Formatted	David Bacon	1/10/2006 1:27:00 PM
42	Font: 12 pt, Bold, No underline, Complex Script Font: 12 pt		
43	Page 14: [56] Formatted	David Bacon	1/10/2006 1:27:00 PM
44	Font: 12 pt, Bold, Complex Script Font: 12 pt		
45	Page 14: [57] Formatted	David Bacon	1/10/2006 1:27:00 PM
46	Font: 12 pt, Bold, No underline, Complex Script Font: 12 pt		
47	Page 14: [58] Formatted	David Bacon	1/10/2006 1:27:00 PM
48	Font: 12 pt, Bold, Complex Script Font: 12 pt		
49	Page 14: [59] Formatted	David Bacon	1/10/2006 1:27:00 PM
50	Font: 12 pt, Complex Script Font: 12 pt		
51	Page 14: [58] Change	OSETSKIYXPLAP	10/13/2005 12:11:00 AM
52	Formatted Bullets and Numbering		
53	Page 14: [59] Change	David Bacon	10/12/2005 7:46:00 PM
54	Formatted Bullets and Numbering		
55	Page 14: [60] Formatted	David Bacon	1/10/2006 1:27:00 PM
56			
57			
58			
59			
60			

1
2
3
4
5
6
7
8
9
10
11
12
13
14
15
16
17
18
19
20
21
22
23
24
25
26
27
28
29
30
31
32
33
34
35
36
37
38
39
40
41
42
43
44
45
46
47
48
49
50
51
52
53
54
55
56
57
58
59
60

Font: 12 pt, Complex Script Font: 12 pt

Page 14: [61] Change	OSETSKIYYNXPLAP	10/13/2005 12:13:00 AM
-----------------------------	------------------------	-------------------------------

Formatted Bullets and Numbering

Page 14: [62] Formatted	David Bacon	1/10/2006 1:27:00 PM
--------------------------------	--------------------	-----------------------------

Font: 12 pt, Complex Script Font: 12 pt

Page 14: [63] Formatted	David Bacon	1/10/2006 1:27:00 PM
--------------------------------	--------------------	-----------------------------

Font: 12 pt, Complex Script Font: 12 pt

Page 14: [64] Formatted	David Bacon	1/10/2006 1:27:00 PM
--------------------------------	--------------------	-----------------------------

Font: 12 pt, No underline, Complex Script Font: 12 pt

Page 14: [65] Formatted	David Bacon	1/10/2006 1:27:00 PM
--------------------------------	--------------------	-----------------------------

Font: 12 pt, Complex Script Font: 12 pt

Page 14: [66] Formatted	David Bacon	1/10/2006 1:27:00 PM
--------------------------------	--------------------	-----------------------------

Font: 12 pt, Not Italic, Complex Script Font: 12 pt

Page 14: [67] Formatted	David Bacon	1/10/2006 1:27:00 PM
--------------------------------	--------------------	-----------------------------

Font: 12 pt, Complex Script Font: 12 pt

Page 14: [68] Formatted	David Bacon	1/10/2006 1:27:00 PM
--------------------------------	--------------------	-----------------------------

Complex Script Font: 12 pt

Page 14: [69] Deleted	David Bacon	10/12/2005 7:46:00 PM
------------------------------	--------------------	------------------------------

D.J. Bacon, Yu.N. Osetsky and Z. Rong, unpublished work.

Yu.N. Osetsky and D.J. Bacon, unpublished work.

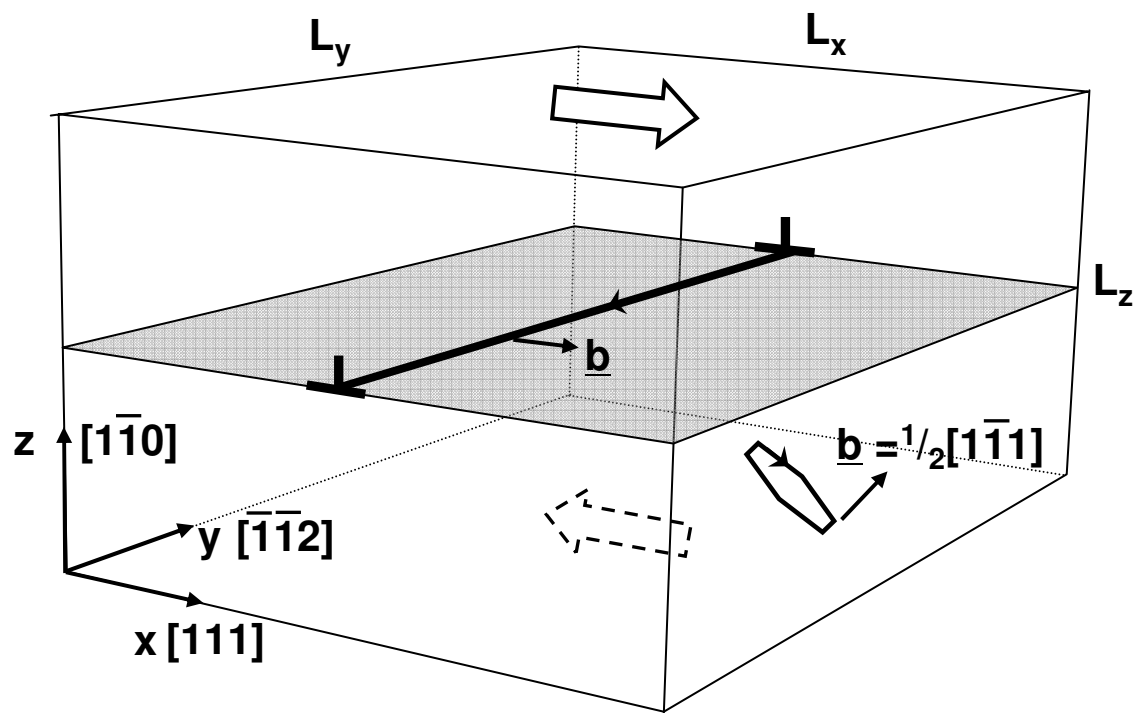
DAVID _ I did not find references to the two last papers?

Page 14: [70] Formatted	David Bacon	10/12/2005 8:12:00 PM
--------------------------------	--------------------	------------------------------

Line spacing: 1.5 lines

<http://mc.manuscriptcentral.com/pm-pml>

1
2
3
4
5
6
7
8
9
10
11
12
13
14
15
16
17
18
19
20
21
22
23
24
25
26
27
28
29
30
31
32
33
34
35
36
37
38
39
40
41
42
43
44
45
46
47
48
49
50
51
52
53
54
55
56
57
58
59
60



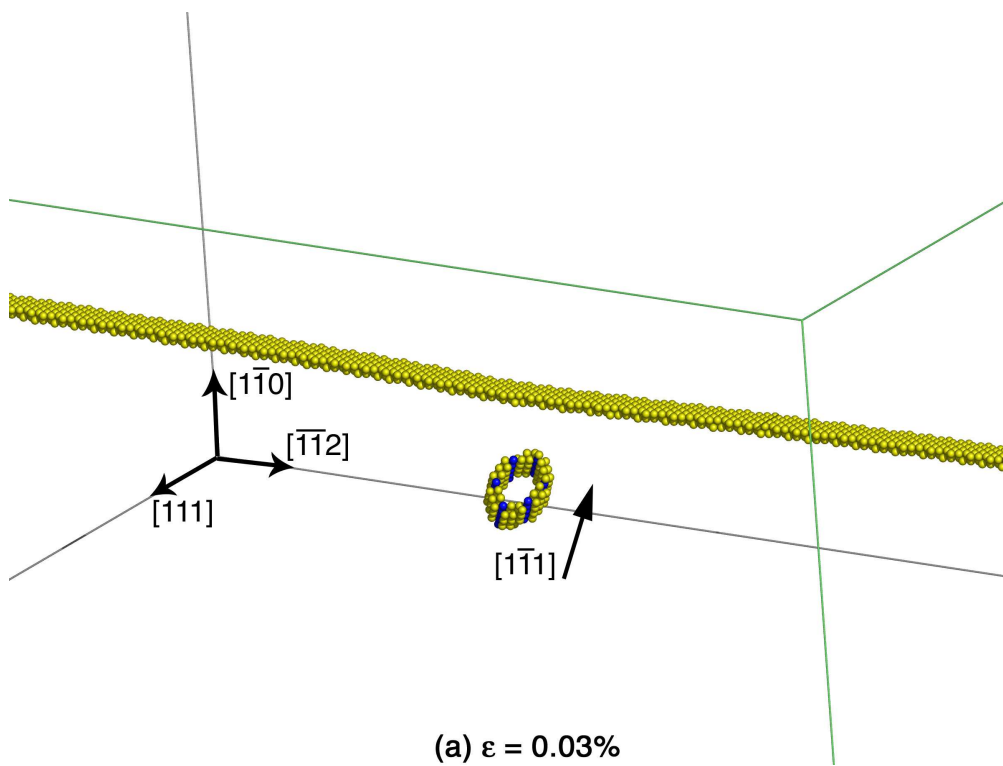
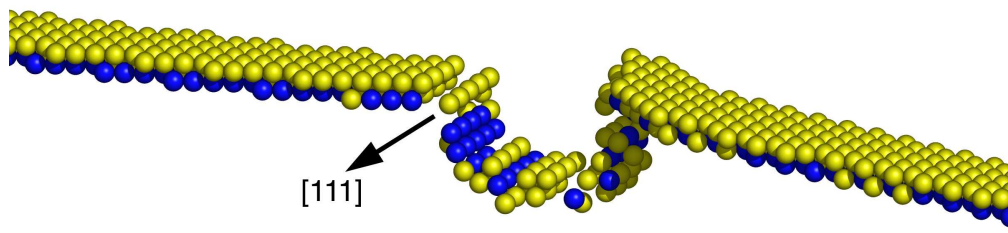


Figure 2a
846x635mm (72 x 72 DPI)

ew Only

1
2
3
4
5
6
7
8
9
10
11
12
13
14
15
16
17
18
19
20
21
22
23
24
25
26
27
28
29
30
31
32
33
34
35
36
37
38
39
40
41
42
43
44
45
46
47
48
49
50
51
52
53
54
55
56
57
58
59
60

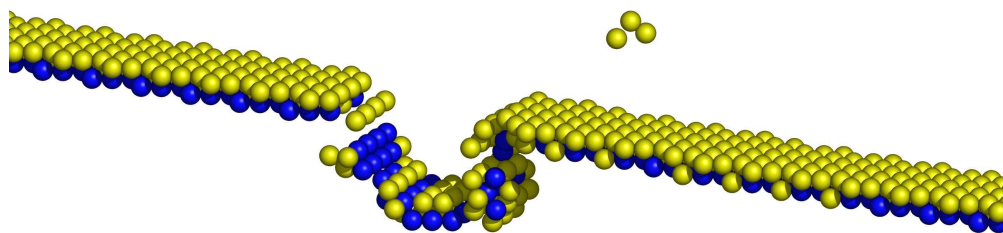
1
2
3
4
5
6
7
8
9
10
11
12
13
14
15
16
17
18
19
20
21
22
23
24
25
26
27
28
29
30
31
32
33
34
35
36
37
38
39
40
41
42
43
44
45
46
47
48
49
50
51
52
53
54
55
56
57
58
59
60



(b) $\epsilon = 0.214\%$

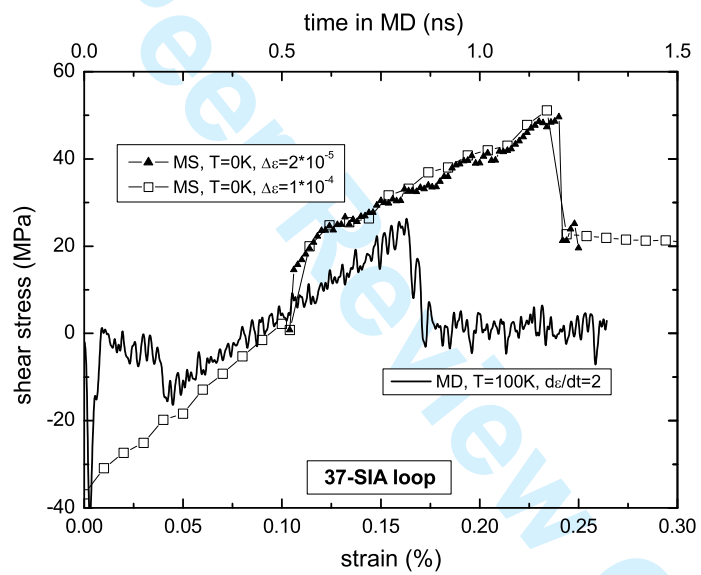
Figure 2b
846x635mm (72 x 72 DPI)

ew Only



(c) $\epsilon = 0.234\%$

Figure 2c
846x635mm (72 x 72 DPI)



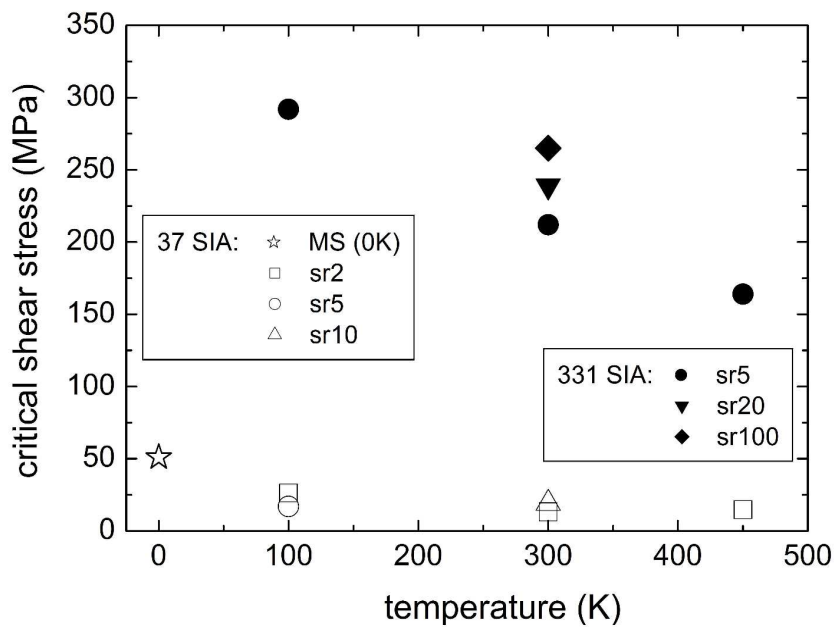
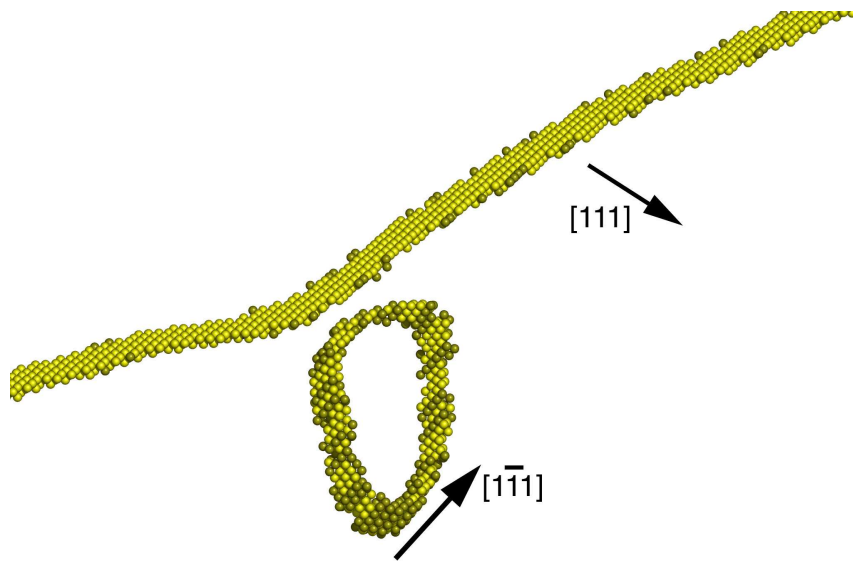


Figure 4
352x245mm (489 x 489 DPI)

View Only

1
2
3
4
5
6
7
8
9
10
11
12
13
14
15
16
17
18
19
20
21
22
23
24
25
26
27
28
29
30
31
32
33
34
35
36
37
38
39
40
41
42
43
44
45
46
47
48
49
50
51
52
53
54
55
56
57
58
59
60

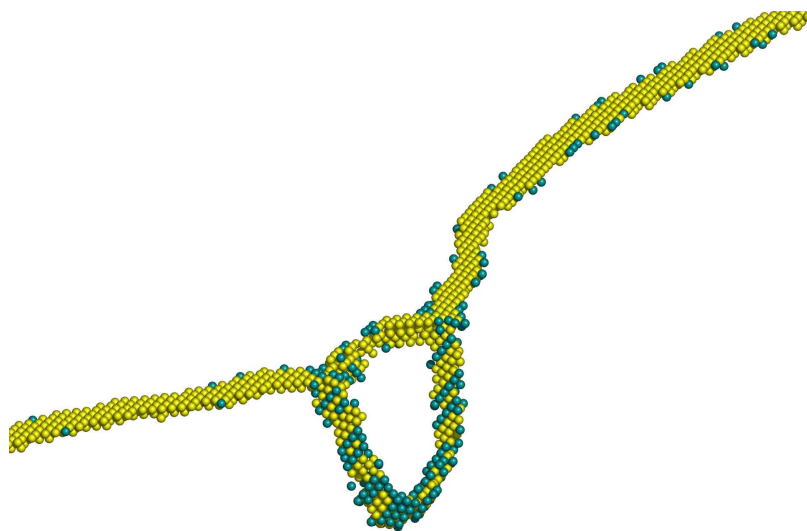


(a) $t = 50\text{ps}$

Figure 5a
846x635mm (72 x 72 DPI)

ew Only

1
2
3
4
5
6
7
8
9
10
11
12
13
14
15
16
17
18
19
20
21
22
23
24
25
26
27
28
29
30
31
32
33
34
35
36
37
38
39
40
41
42
43
44
45
46
47
48
49
50
51
52
53
54
55
56
57
58
59
60



(b) $t = 55\text{ps}$

Figure 5b
846x635mm (72 x 72 DPI)

ew Only

1
2
3
4
5
6
7
8
9
10
11
12
13
14
15
16
17
18
19
20
21
22
23
24
25
26
27
28
29
30
31
32
33
34
35
36
37
38
39
40
41
42
43
44
45
46
47
48
49
50
51
52
53
54
55
56
57
58
59
60

1
2
3
4
5
6
7
8
9
10
11
12
13
14
15
16
17
18
19
20
21
22
23
24
25
26
27
28
29
30
31
32
33
34
35
36
37
38
39
40
41
42
43
44
45
46
47
48
49
50
51
52
53
54
55
56
57
58
59
60

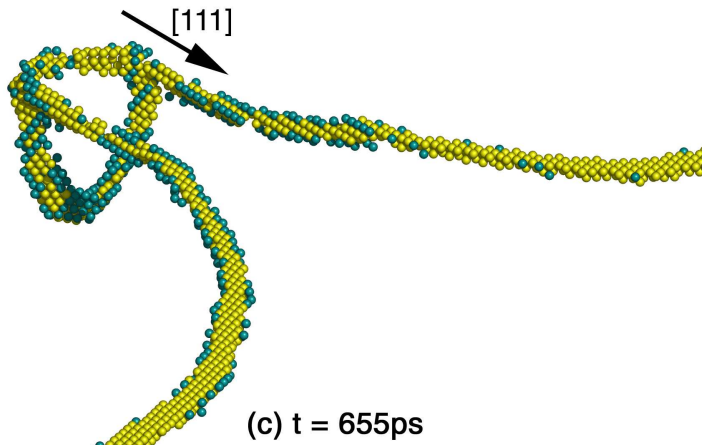
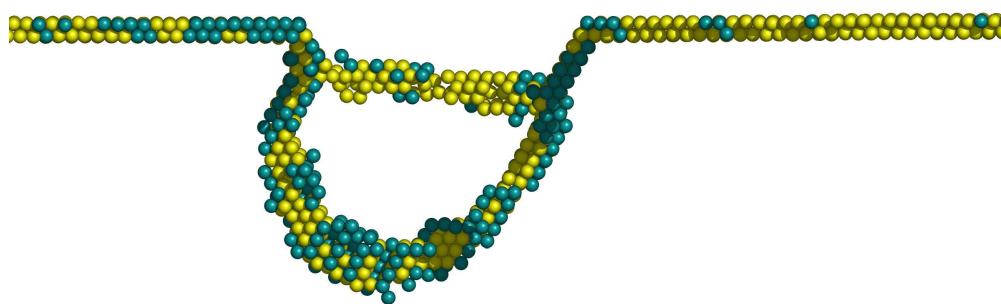


Figure 5c
846x635mm (72 x 72 DPI)

ew Only



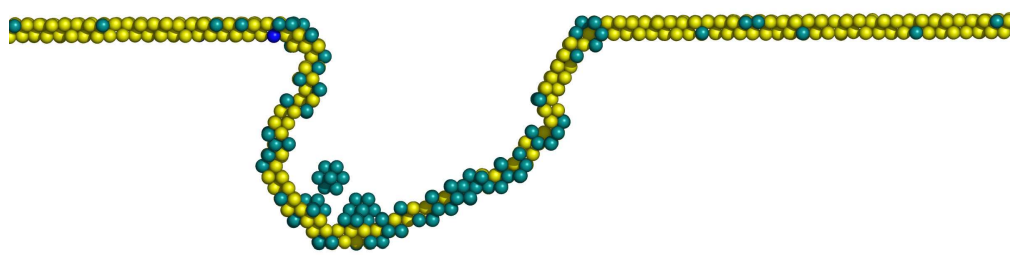
(d) $t = 655\text{ps}$

Figure 5d
846x635mm (72 x 72 DPI)

ew Only

1
2
3
4
5
6
7
8
9
10
11
12
13
14
15
16
17
18
19
20
21
22
23
24
25
26
27
28
29
30
31
32
33
34
35
36
37
38
39
40
41
42
43
44
45
46
47
48
49
50
51
52
53
54
55
56
57
58
59
60

1
2
3
4
5
6
7
8
9
10
11
12
13
14
15
16
17
18
19
20
21
22
23
24
25
26
27
28
29
30
31
32
33
34
35
36
37
38
39
40
41
42
43
44
45
46
47
48
49
50
51
52
53
54
55
56
57
58
59
60

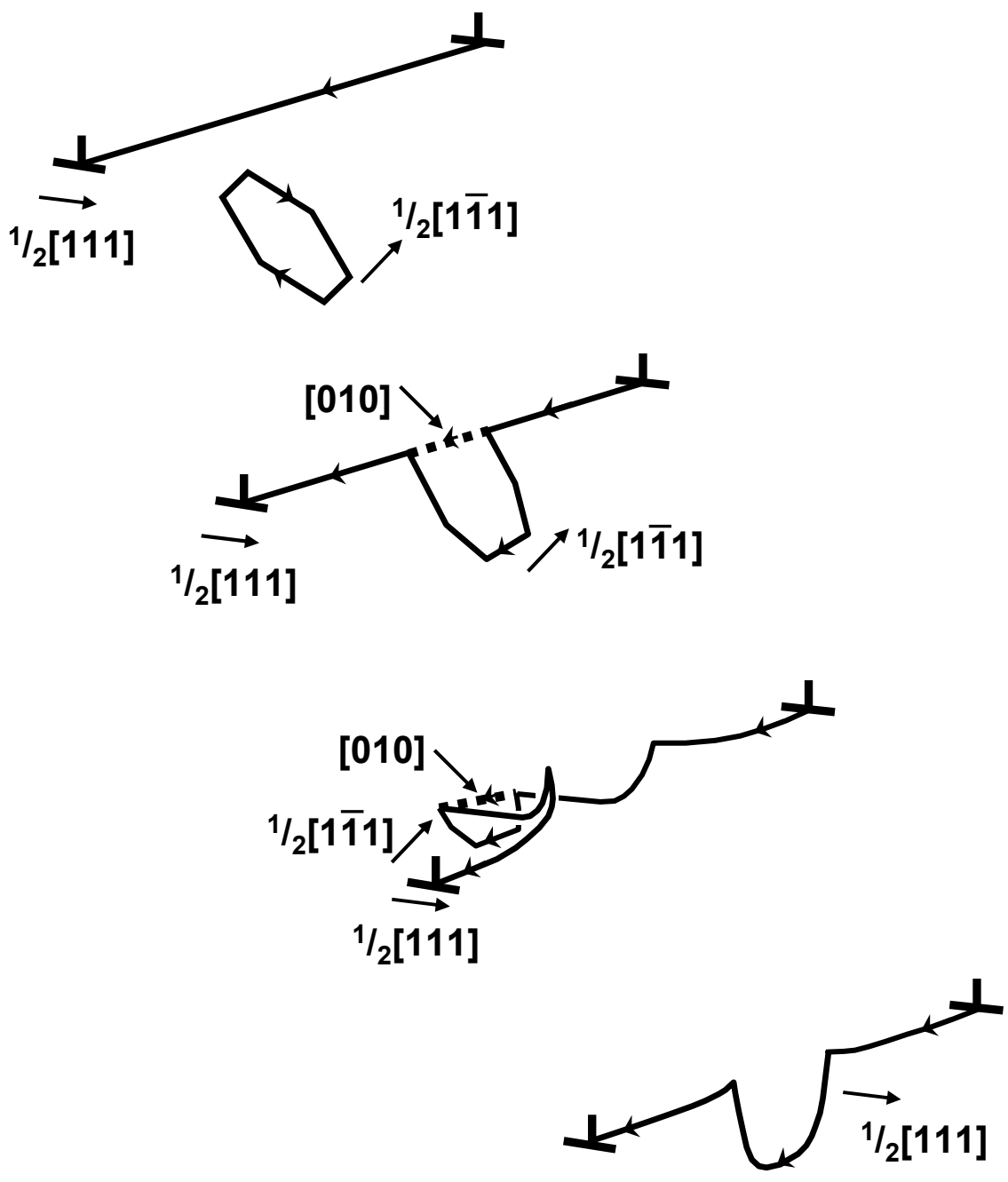


(e) $t = 765\text{ps}$

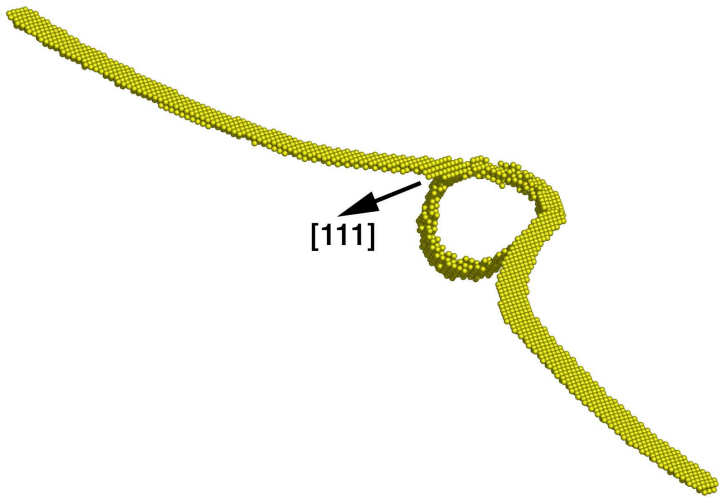
Figure 5e
846x635mm (72 x 72 DPI)

ew Only

1
2
3
4
5
6
7
8
9
10
11
12
13
14
15
16
17
18
19
20
21
22
23
24
25
26
27
28
29
30
31
32
33
34
35
36
37
38
39
40
41
42
43
44
45
46
47
48
49
50
51
52
53
54
55
56
57
58
59
60



1
2
3
4
5
6
7
8
9
10
11
12
13
14
15
16
17
18
19
20
21
22
23
24
25
26
27
28
29
30
31
32
33
34
35
36
37
38
39
40
41
42
43
44
45
46
47
48
49
50
51
52
53
54
55
56
57
58
59
60



(a) $t = 1.4\text{ns}$, $\tau = 95\text{MPa}$

Figure 7a
846x635mm (72 x 72 DPI)

iew Only



Figure 7b
849x593mm (72 x 72 DPI)

View Only

1
2
3
4
5
6
7
8
9
10
11
12
13
14
15
16
17
18
19
20
21
22
23
24
25
26
27
28
29
30
31
32
33
34
35
36
37
38
39
40
41
42
43
44
45
46
47
48
49
50
51
52
53
54
55
56
57
58
59
60

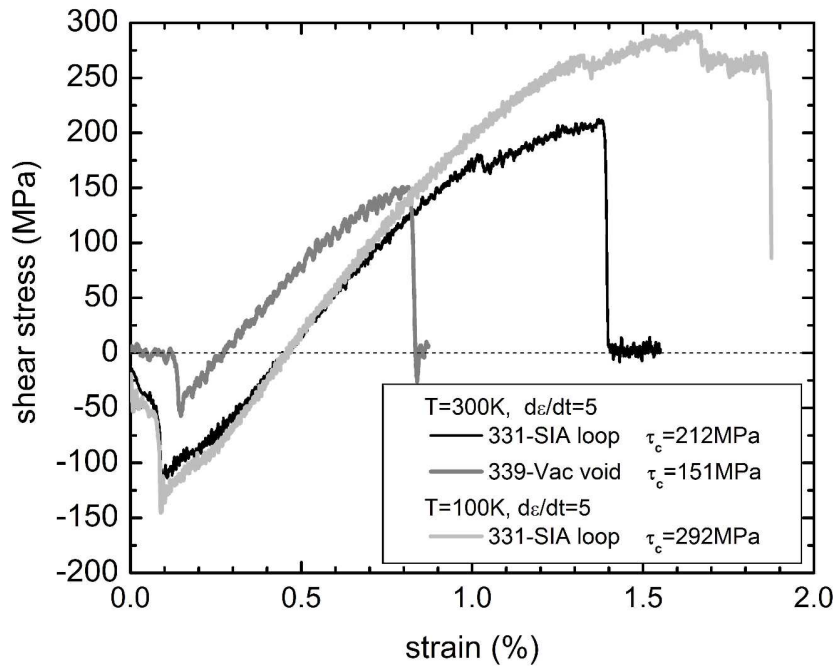


Figure 8
331x254mm (490 x 490 DPI)

Pre-proof Only